iScience

CellPress
OPEN ACCESS

Article

Applying machine learning to balance performance and stability of high energy density materials

Xiaona Huang, Chongyang Li, Kaiyuan Tan, ..., Chang Q. Sun, Michael Gozin, Lei Zhang

wenys@caep.cn (Y.W.)
fengguo@lcu.edu.cn (F.G.)
cogozin@gmail.com (M.G.)
zhang_lei@iapcm.ac.cn (L.Z.)

HIGHLIGHTS

Crystal-level quantum mechanics calculations of 21,648 physicochemical data of 153 HEDMs

Machine learning of detonation and stability of HEDMs and experimental validation

Data-driven insight into the causality of performance-stability contradiction

Optimal range of key features for rational design of advanced HEDMs

Huang et al., iScience *24*, 102240
March 19, 2021
https://doi.org/10.1016/j.isci.2021.102240

iScience

CellPress
OPEN ACCESS

Article

Applying machine learning to balance performance and stability of high energy density materials

Xiaona Huang,[1,2,3,12] Chongyang Li,[2,4,12] Kaiyuan Tan,[1] Yushi Wen,[1,*] Feng Guo,[5,*] Ming Li,[1] Yongli Huang,[2] Chang Q. Sun,[6,7] Michael Gozin,[8,9,10,*] and Lei Zhang[2,11,13,*]

SUMMARY

The long-standing performance-stability contradiction issue of high energy density materials (HEDMs) is of extremely complex and multi-parameter nature. Herein, machine learning was employed to handle 28 feature descriptors and 5 properties of detonation and stability of 153 HEDMs, wherein all 21,648 data used were obtained through high-throughput crystal-level quantum mechanics calculations on supercomputers. Among five models, namely, extreme gradient boosting regression tree (XGBoost), adaptive boosting, random forest, multi-layer perceptron, and kernel ridge regression, were respectively trained and evaluated by stratified sampling and 5-fold cross-validation method. Among them, XGBoost model produced the best scoring metrics in predicting the detonation velocity, detonation pressure, heat of explosion, decomposition temperature, and lattice energy of HEDMs, and XGBoost predictions agreed best with the 1,383 experimental data collected from massive literatures. Feature importance analysis was conducted to obtain data-driven insight into the causality of the performance-stability contradiction and delivered the optimal range of key features for more efficient rational design of advanced HEDMs.

INTRODUCTION

High energy density materials (HEDMs), also known as energetic materials, mainly refer to explosives, propellants, and pyrotechnics depending on their properties, formulations, and intended applications (Agrawal, 2010). As an alternative way to the use of human work, utilization of HEDMs alleviates arduous tasks of quarrying, mining, building tunnels, taming rivers, and building roads/rails by quick release of large amounts of gas through controlled chemical reactions, making laborious activities more efficient and economical, thereby playing an important role in accelerating the progress of human civilization (Klapötke, 2015). In this modern era, the dramatic increase in global population and concomitant depletion of available resources are demanding more advanced HEDMs to safely explore ultra-deep mineral deposits of earth, conduct space exploration, and so forth. Nonetheless, the development of HEDMs has been an incredibly slow process, with its milestones being the discovery of black powder at around 220 BC, the invention of trinitrotoluene (TNT) in the 1880s, the synthesis of widely used octahydro-1,3,5,7-tetranitro-1,3,5,7-tetrazocine (HMX) during World War II, and the development 2,4,6,8,10,12-hexanitro-2,4,6,8,10,12-hexaazatetracyclo-[5.5.0.0^{3,11}.0^{5,9}]-dodecane (CL-20) in 1980s. The currently required capability of HEDMs demands high detonation performance (maximum detonation velocity D, maximum detonation pressure $p_{C\text{-}J}$, and maximum heat of explosion Q_{max}) with simultaneous maximum stability, which includes minimal chemical degradation upon storage, no phase transition to a polymorph with an inferior performance, and no initiation upon accidental mechanical impact, friction, and non-mechanical *stimuli*, such as exposure to light, to irradiation in a non-visible spectral range, to electrostatic discharge, etc. Unfortunately, currently used state-of-the-art HEDMs have difficulty in addressing in a satisfactory manner all these conflicting criteria.

Possibly, the extremely high hazard involved and the high cost of the experimental research on HEDMs, as well as the long-term life cycle of their characterization, manufacturing, testing, and inspection, could be the excuses for the slow development of HEDMs (Wejsa, 2014). Furthermore, one more important reason for the slow development of HEDMs is the contradiction between their high detonation performance and high stability (Shukla et al., 2017; Sabin, 2014; Yu et al., 2020; Zhang et al., 2014; Tang et al., 2020; Jiao et al., 2018). A high detonation performance of HEDMs relies on the large energy difference between the reactants and the reaction products, whereas the high stability of HEDMs requires a sufficiently high energy barrier to prevent the uncontrolled

[1]Institute of Chemical Materials, China Academy of EngineeringPhysics (CAEP), Mianyang, 621900, China

[2]CAEP Software Center for High Performance Numerical Simulation, Beijing, 100088, China

[3]Department of Mechanical Engineering, City University of Hong Kong, 83 Tat Chee Avenue, Kowloon, 999077, Hong Kong, China

[4]Key Laboratory of Low-dimensional Materials and Application Technology (Ministry of Education), School of Materials Science and Engineering, Xiangtan University, Xiangtan, 411105, China

[5]School of Physical Science and Information Technology, Liaocheng University, Liaocheng, 252000, China

[6]EBEAM, Yangtze Normal University, Chongqing, 408100, China

[7]NOVITAS, Nanyang Technological University, Singapore, 639798, Singapore

[8]School of Chemistry, Faculty of Exact Science, Tel Aviv University, Tel Aviv, 69978, Israel

[9]Tel Aviv University Center for Nanoscience and Nanotechnology, Tel Aviv, 69978, Israel

[10]Center of Advanced Combustion Science, Tel Aviv University, Tel Aviv, 69978, Israel

[11]Laboratory of Computational Physics, Institute of Applied Physics and Computational Mathematics, Beijing, 100088, China

[12]These authors contributed equally

[13]Lead contact

*Correspondence: wenys@caep.cn (Y.W.), fengguo@lcu.edu.cn (F.G.),

Continued

initiation of such reactions (Jiao et al., 2018). Known molecular design strategies in reaching high detonation performance of HEDMs, in many perspectives, conflict with those in reaching high stability. For example, the presence of nitro group, N-oxide group, nitramino, furazan, furoxan, or oxadiazole in energetic molecules can increase the oxygen balance (OB) of HEDMs; and incorporation of azido group, N = C, and N = N bonds into energetic molecules can lead to the increase in the nitrogen content (ρ_N) of HEDMs (Yu et al., 2020). Both strategies were capable of leading to the increase of the density (ρ) and heat of formation of the energetic molecules, facilitating the promotion of their detonation performance (Hu et al., 2020). However, when the increase in the OB leads to better performance, it pays the price of higher sensitivity and lower stability of the resulting HEDM (Wang et al., 2018; Li et al., 2020a, 2020b, 2020c). Moreover, the increase of ρ_N in various nitrogen-rich HEDMs inevitably introduces N–N bonds, the low bond strength of which would result in reduced stability of such molecules (Tang et al., 2017; Zong et al., 2020).

Besides the aforementioned factors, numerous crystal-level physicochemical parameters, such as intermolecular interactions, energetics of the compound, crystal packing arrangements, and ratio of component molecules in co-crystals, were also found to significantly influence the detonation performance and stability of HEDMs. For example, hydrogen bonding (HB) plays a vital role in optimizing both detonation performance and crystal stability. Crystal structures of HEDMs rich in HBs were shown to have better stability, and expressed enhanced heat resistance and improved insensitivity to impact and shock *stimuli*, versus compounds with limited HB amount in their crystal structures (Rupeng et al., 2019; Li et al., 2020a, 2020b, 2020c; Zhang et al., 2019a, 2019b, 2019c, 2019d). For example, when compared with neutral tetranitroamino HEDMs, corresponding energetic salts showed better thermal and mechanical stabilities, owing to the extensive HB interactions between cations and anions (Lang et al., 2020). However, unfortunately, high content of hydrogen in energetic molecules would in turn lead to decreased ρ and reduced detonation performance of HEDMs.

Over the past decade, the machine learning (ML) algorithms have emerged, rapidly developed, and been extensively used in materials research (Zahrt et al., 2019; Sanchez-Lengeling and Aspuru-Guzik, 2018; Lu et al., 2018; Zhong et al., 2020; Granda et al., 2018; Butler et al., 2018). Compared with the traditional physics-based or knowledge-driven approach, ML algorithms are data driven and have an important characteristic trait of easily handling very complex datasets, providing accurate predictions, and helping in deciphering new knowledge (Shi and Iyengar, 2020). Therefore, ML is an extremely promising technique to handle the detonation-stability contradiction conundrum and accelerate the progress in the design of advanced HEDMs.

Noteworthy, reasonable feature descriptors and suitable models are the key to the successful application of the ML tool in solving the detonation-stability contradiction. According to the literature, commonly employed feature descriptors of HEDMs are the structure and energy properties of individual molecules, rather than those of crystals, owing to the lack of a reliable quantum chemical approach to handle the periodic structures of crystals and the weak in-crystal intermolecular interactions. In general, the feature descriptors include counts of atoms, bonds, and groups; OB; nitrogen-to-carbon ratio; bond types; electro-topological state; fingerprinting; Coulomb matrices; highest occupied and lowest unoccupied molecular orbitals; nitrogen charges at the bond midpoint; the lowest negative charge on nitro group; molecular polarizability; ionization energy; etc. (Elton et al., 2018; Barnes et al., 2018; Wang et al., 2012; Zhang et al., 2017; Cho et al., 2005; Kang et al., 2020). A considerable part of these feature descriptors is quantum chemical calculation results for HEDM molecules. Till date, the models that have been designed, developed, and employed for ML of HEDMs include multiple linear regression, artificial neural network (ANN), kernel ridge regression (KRR), support vector regression, random forest (RF), *k*-nearest neighbors, decision tree, least absolute shrinkage, selection operator regression, Gaussian process regression, etc. (Xu et al., 2012; Wang et al., 2012; Fathollahi and Sajady, 2018; Elton et al., 2018; Barnes et al., 2018; Kang et al., 2020; Zhang et al., 2017; Chandrasekaran et al., 2019; Nefati et al., 1996). The validation metrics derived from these data-driven models brought a high confidence in their use for a reasonably reliable prediction of D, $p_{C\text{-}J}$, Q_{max}, heat of formation, impact sensitivity, decomposition temperature (T_d), and other critical properties of HEDMs (Xu et al., 2012; Wang et al., 2012; Fathollahi and Sajady, 2018; Elton et al., 2018; Barnes et al., 2018, Barnes et al., 2020; Kang et al., 2020; Gupta et al., 2016; Chandrasekaran et al., 2019; Nefati et al., 1996).

In this study, we made an effort to bridge the gap that exists between the nature of discrete molecule and extended periodic solid material (Mancuso et al., 2020) by conducting quantum mechanics calculations on parameters of physicochemical properties of 153 HEDMs, directly at the crystal level, instead of more common calculations dealing with individual molecules in a gas phase. These 21,648 calculated data were then

cogozin@gmail.com (M.G.),
zhang_lei@iapcm.ac.cn (L.Z.)

https://doi.org/10.1016/j.isci.2021.102240

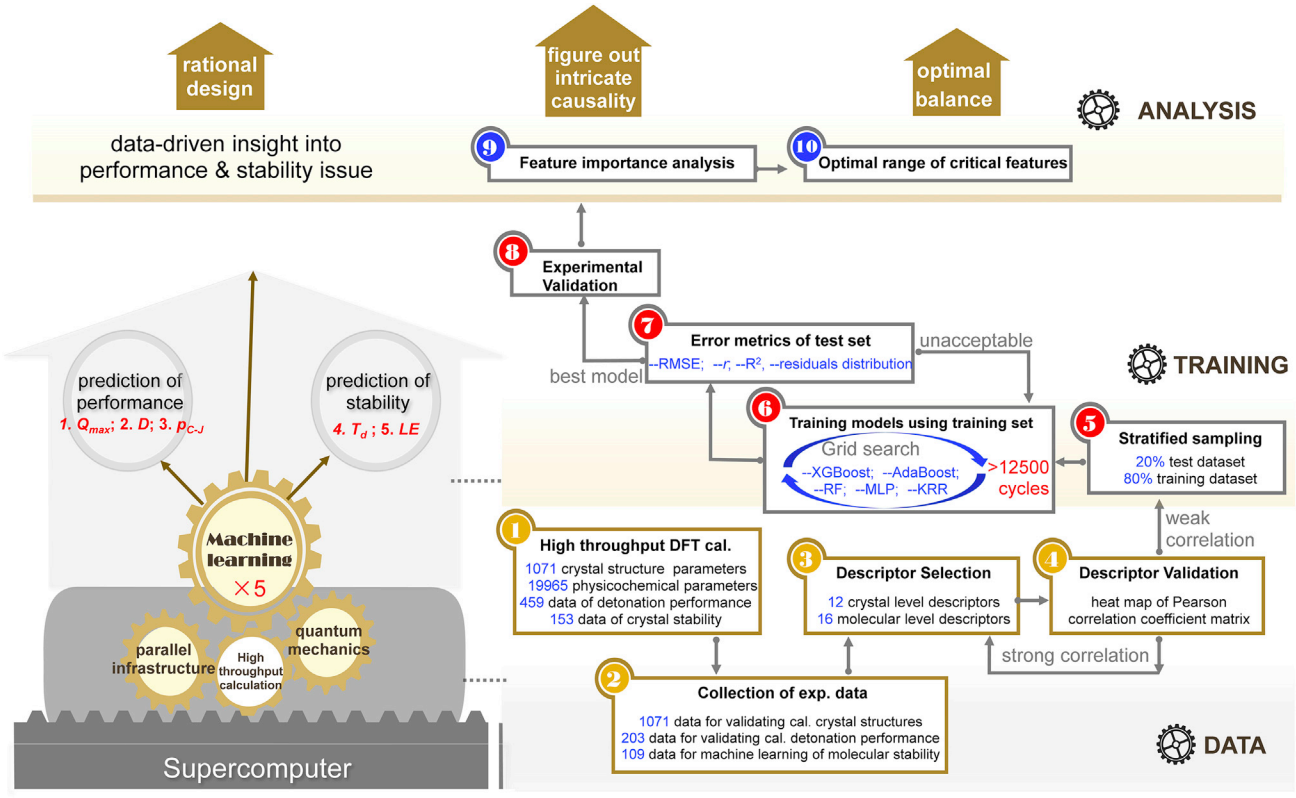

Figure 1. A flow chart of ML process for balancing detonation performance and stability of HEDMs

High-throughput DFT calculations on supercomputers are the basis of data preparation for ML. Five ML models were trained and evaluated using stratified sampling and leave-one-out cross-validation, and the collected massive experimental data help to validate the predictions. Feature importance ranking provides a data-driven insight into the performance-stability contradiction and presents guidance on the optimal range of critical features.

used as input for ML. Five models were, respectively, trained and evaluated in predicting the D, $p_{C\text{-}J}$, Q_{max}, T_d, and lattice energy (LE) of HEDMs; 1,383 experimental data were collected from a comprehensive literature search to verify the reliability of our current calculations and ML predictions. Subsequently, feature importance analysis was carried out; the features were classified into contradictory and non-contradictory categories, and finally the optimal range of key features was recommended for use in a rational molecular design of novel advanced HEDMs.

RESULTS

Materials informatics and machine learning

Figure 1 shows a flow chart of the use of ML technique for addressing the contradiction between detonation performance and stability of HEDMs. Current study concentrates on 153 reported HEDMs, which are all stable at ambient conditions, and their single-crystal X-ray crystallography data are available. The physicochemical parameters, detonation performance parameters, and stability properties were calculated at the crystal level, by using a recently developed density functional theory (DFT) software, high accuracy atomistic simulation package for energetic materials (HASEM) (Zhang et al., 2016a, 2016b). J parallel adaptive structured mesh applications infrastructure (JASMIN) facilitates HASEM to adapt to modern supercomputers, thereby allowing high-throughput DFT calculations (Mo et al., 2010). The lattice parameters and atomic coordinates from the experimental data were set as the input of HASEM software to optimize structures. Minute discrepancies between the calculated and experimental results of 1,071 crystal structure parameters confirm the high reliability of HASEM method in describing the crystal structures of HEDMs (Figure 2).

Dataset

Based on these optimized structures, 19,965 physicochemical parameters were calculated and employed as feature descriptor candidates for ML of HEDMs (Tables 1 and S2). Furthermore, 459 calculated values of

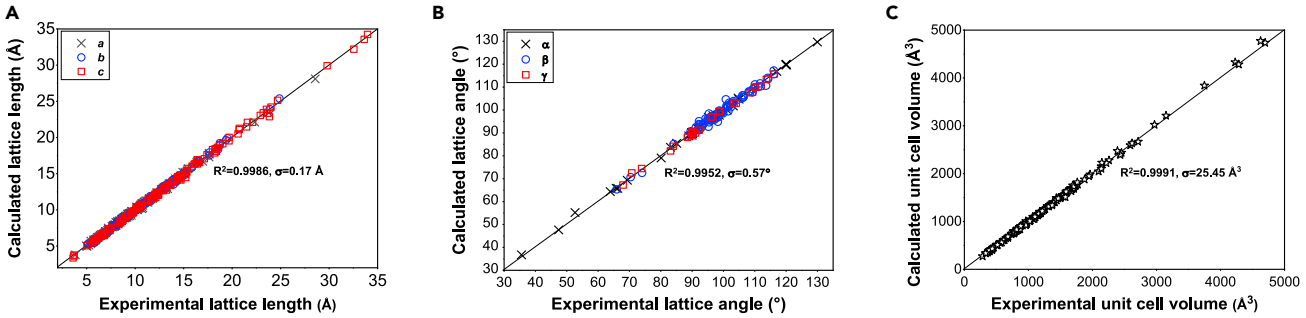

Figure 2. DFT calculation of 1,071 crystal structure parameters of HEDMs studied herein and their experimental validation

(A–C) (A) Lattice constants (*a*, *b*, and *c*); (B) lattice angles (α, β, and γ); and (C) unit cell volumes of the 153 HEDMs studied.

D, $p_{C\text{-}J}$, and Q_{max}; 153 calculated values of *LE*; and 109 collected experimental data of T_d were used as outcomes to train the ML models for predicting the detonation performance, crystal stability, and molecular stability of HEDMs, respectively. Additional 203 collected experimental data were used to validate the results of ML predictions (Table S3; supplemental information).

For each of the studied 153 HEDMs, the compound name; its molecular formula, diagram, and conformation; as well as the Cambridge Crystallographic Data Center (CCDC) index number and Chemical Abstracts Service (CAS) number are provided in the Table S3 presented in the supplemental information. Details of our calculation methods of various physicochemical parameters and properties are described in our previous reports (Zhang et al., 2016a, 2016b, 2019a, 2019b, 2019c, 2019d; Jiang et al., 2018; He et al., 2017).

In each ML process for the prediction of *D*, $p_{C\text{-}J}$, Q_{max}, T_d, and *LE*, the dataset was divided into a training dataset (80%) and a test dataset (20%), in which stratified sampling was conducted to reduce sampling error and to improve the performance of ML.

Feature descriptors

All calculated physicochemical parameters were classified into crystal level and molecular level groups. The *crystal level parameters* include space group, number of molecules in one primitive cell, packing types, packing coefficient (PC), ρ, ρ_N, OB, intermolecular HB count, intermolecular HB strength, intermolecular HB length, and in-crystal mixture with hydrogen-rich molecules or energetic molecules. The *molecular level parameters* include shape of molecular backbones; molecular weight (MW); intramolecular bond length; intramolecular bond strength; number of critical functional groups, such as $-NO_2$, $-NH_2$, –OH, $-CH_3$, and $-N_3$; as well as the distribution of detonation products, including gaseous CO_2, H_2O, N_2, O_2, and NH_3 and solid C. Although part of the calculated data for 118 HEDMs was mentioned in our recent studies (Li et al., 2020a, 2020b, 2020c), in the present work, the calculated data of physicochemical parameters for these compounds were significantly increased and further DFT calculations for additional 35 HEDMs were performed to enlarge the dataset.

Among the 5,941 intermolecular HB and intramolecular bonds studied, the strongest intermolecular HB for each HEDM and its weakest intramolecular chemical bond were screened out and used as feature descriptors of the HEDM compound (Tables S1 and S2; supplemental information). Eventually, 28 types of feature descriptors were selected for the following ML study.

Furthermore, Pearson correlation coefficient matrices were calculated to identify the positive and negative correlations between pairs of selected features, as shown in Figure 3. The low linear correlations for the feature descriptors indicate that redundant and irrelevant features were not included in current study, which helps improve ML performance.

Model training

An appropriate model and its optimized hyperparameters constitute crucial preconditions for the successful application of ML in molecular and materials research. Herein, five representative ML models, including

Table 1. Scoring metrics of the 5 ML models in predicting detonation and stability properties (D, $p_{C\text{-}J}$, Q_{max}, T_d, and LE) of HEDMs, provided individually for the training set and test set

			Training dataset			Test dataset		
Properties		Models	RMSE	r	R^2	RMSE	R	R^2
Detonation performance	Q_{max}	XGBoost	49.694	0.984	0.958	99.988	0.914	0.825
		AdaBoost	60.579	0.970	0.938	108.252	0.898	0.794
		RF	55.731	0.983	0.948	103.574	0.926	0.812
		MLP	78.539	0.947	0.896	101.070	0.909	0.821
		KRR	96.939	0.918	0.841	101.291	0.916	0.820
	D	**XGBoost**	**0.101**	**0.993**	**0.985**	**0.235**	**0.956**	**0.912**
		AdaBoost	0.114	0.991	0.981	0.274	0.942	0.879
		RF	0.143	0.986	0.970	0.276	0.943	0.878
		MLP	0.185	0.976	0.949	0.244	0.959	0.905
		KRR	0.256	0.950	0.903	0.291	0.941	0.864
	$p_{C\text{-}J}$	**XGBoost**	**0.817**	**0.992**	**0.984**	**1.788**	**0.954**	**0.910**
		AdaBoost	1.084	0.987	0.972	2.426	0.920	0.835
		RF	1.097	0.987	0.971	2.360	0.924	0.843
		MLP	0.898	0.990	0.981	2.256	0.954	0.857
		KRR	1.983	0.951	0.905	2.812	0.902	0.778
Molecular stability	T_d	**XGBoost**	**29.919**	**0.933**	**0.803**	**52.069**	**0.781**	**0.557**
		AdaBoost	26.932	0.947	0.840	54.347	0.741	0.518
		RF	21.229	0.970	0.901	54.153	0.728	0.521
		MLP	32.256	0.878	0.770	60.670	0.635	0.399
		KRR	51.152	0.653	0.423	61.573	0.627	0.381
Crystal stability	LE	**XGBoost**	**1.033**	**0.999**	**0.998**	**3.494**	**0.976**	**0.948**
		AdaBoost	3.187	0.990	0.977	6.724	0.898	0.806
		RF	4.281	0.980	0.958	5.497	0.933	0.870
		MLP	3.124	0.989	0.978	6.416	0.917	0.823
		KRR	4.558	0.976	0.952	4.367	0.959	0.918

The best performing results are marked in bold.

extreme gradient boosting regression tree (XGBoost), adaptive boosting regressor (AdaBoost), RF, multi-layer perceptron (MLP), and KRR, were employed.

Subsequently, grid search method was utilized to optimize the hyperparameters of the five models and 5-fold cross-validation method was used to evaluate the error metrics of each model. Herein, the 5 folds were obtained by random division of the training dataset. The cross-validation procedure was carried out 5 times, and the one with the best error metrics aided in the determination of the final hyperparameters of this model. In the entire training process, the grid search and cross-validation loop were conducted for more than 12,500 times in total and 25 sets of optimal hyperparameters in predicting D, $p_{C\text{-}J}$, Q_{max}, T_d, and LE were eventually determined for the 5 models, as shown in Figure 1. While training the MLP model, the fingerprints were standardized, and the Rectified Linear Unit (ReLU) activation function was used. The hidden layer size is (3, 3) in predicting D, Q_{max}, and LE, and is (3, 2) in predicting of T_d and $p_{C\text{-}J}$. While training the KRR models, the polynomial kernel function was used in the prediction of D, $p_{C\text{-}J}$, Q_{max}, and T_d, and the linear kernel function was used in the prediction of LE. The parameters were optimized using the grid search method.

Model inference and validation

To evaluate the robustness of the above-identified hyperparameters and the performance of the five trained models, herein, the prediction errors were estimated by using three scoring metrics, namely,

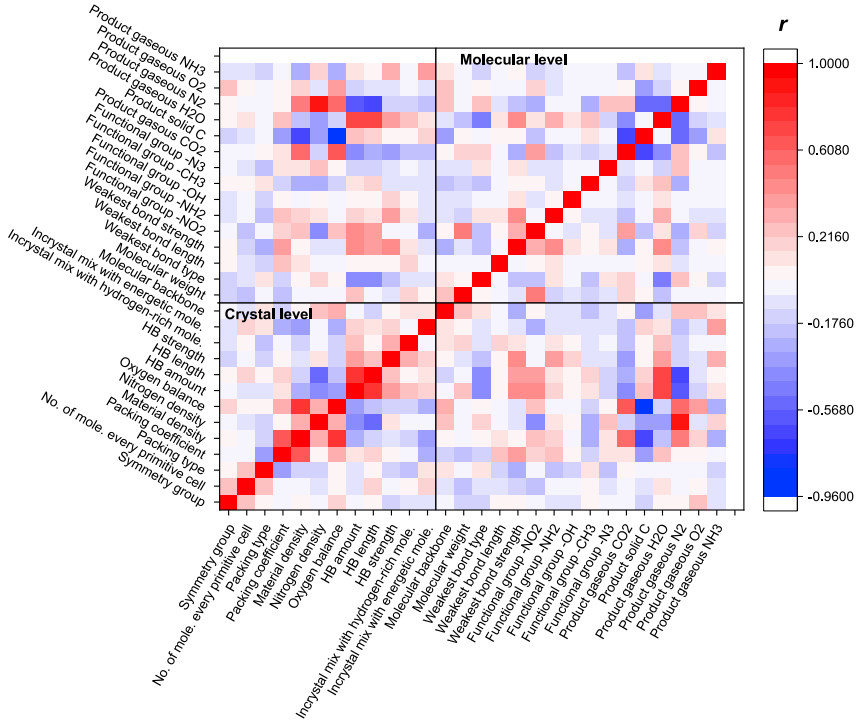

Figure 3. Heatmap of Pearson correlation coefficient of selected features

root-mean-square error (RMSE), Pearson correlation coefficient (r), and coefficient of determination (R^2) and then the distribution of the residuals of the predictions was compared with the normal distributions. The prediction errors were calculated independently for the training set and test set, as presented in Table 1. The performances of the five models in the prediction of D, $p_{C\text{-}J}$, Q_{max}, T_d, and LE are plotted in Figures S1–S21 (Supplemental information), wherein XGBoost exhibits the best performance. The XGBoost predictions of all five properties of the training set and the test set and the distribution of the prediction residuals of the entire set are shown in Figure 4.

Detonation performance characterized based on heat of explosion, detonation velocity, and detonation pressure. The motivation of the current work is to explore the optimal design of advanced HEDMs with simultaneous high detonation performance and high stability, so we consider only the maximum detonation performance, which is calculated at the maximum theoretical density for each of the 153 compounds studied.

For the prediction of Q_{max}, XGBoost model shows the best agreement with the results calculated by the DFT method for the training set ($RMSE$ = 49.69 kcal·kg^{-1}, r = 0.98, and R^2 = 0.96) and the test set ($RMSE$ = 99.99 kcal·kg^{-1}, r = 0.91, and R^2 = 0.82), as summarized in Table 1. Comparative analysis of the distributions of the residuals of the predicted Q_{max} of the five models, as shown in Figures 4B and S2–S5, indicates that XGBoost prediction residuals present the closest distributions to normal distributions. Furthermore, a simple statistic showed that 74.5% of the XGBoost-predicted Q_{max} was comparable to the DFT results with a relative error less than 5%, and 93.5% of the XGBoost predictions showed a relative error below 10%, thereby confirming the accuracy of the XGBoost prediction. Compared with a previous RF prediction of Q_{max} (R^2 = 0.99 for training set and R^2 = 0.93 for test set), current metrics (R^2 = 0.96 for training set and R^2 = 0.82 for test set) are slightly lower; however, our dataset of 153 HEDMs is much larger than the dataset of 41 HEDMs reported by Hong and coworkers (Kang et al., 2020). Our metrics are much better than the KRR predictions of Q_{max} for 109 energetic compounds, wherein r = 0.88 and R^2 = 0.88 for the training set and r = 0.79 and R^2 = 0.76 for the test set (Elton et al., 2018).

Regarding the prediction of D, all the five studied models exhibited pretty good performance, with all the values of $RMSE$ smaller than 0.3 km s^{-1}, all values of r higher than 0.94, and all values of R^2 higher than 0.86, as

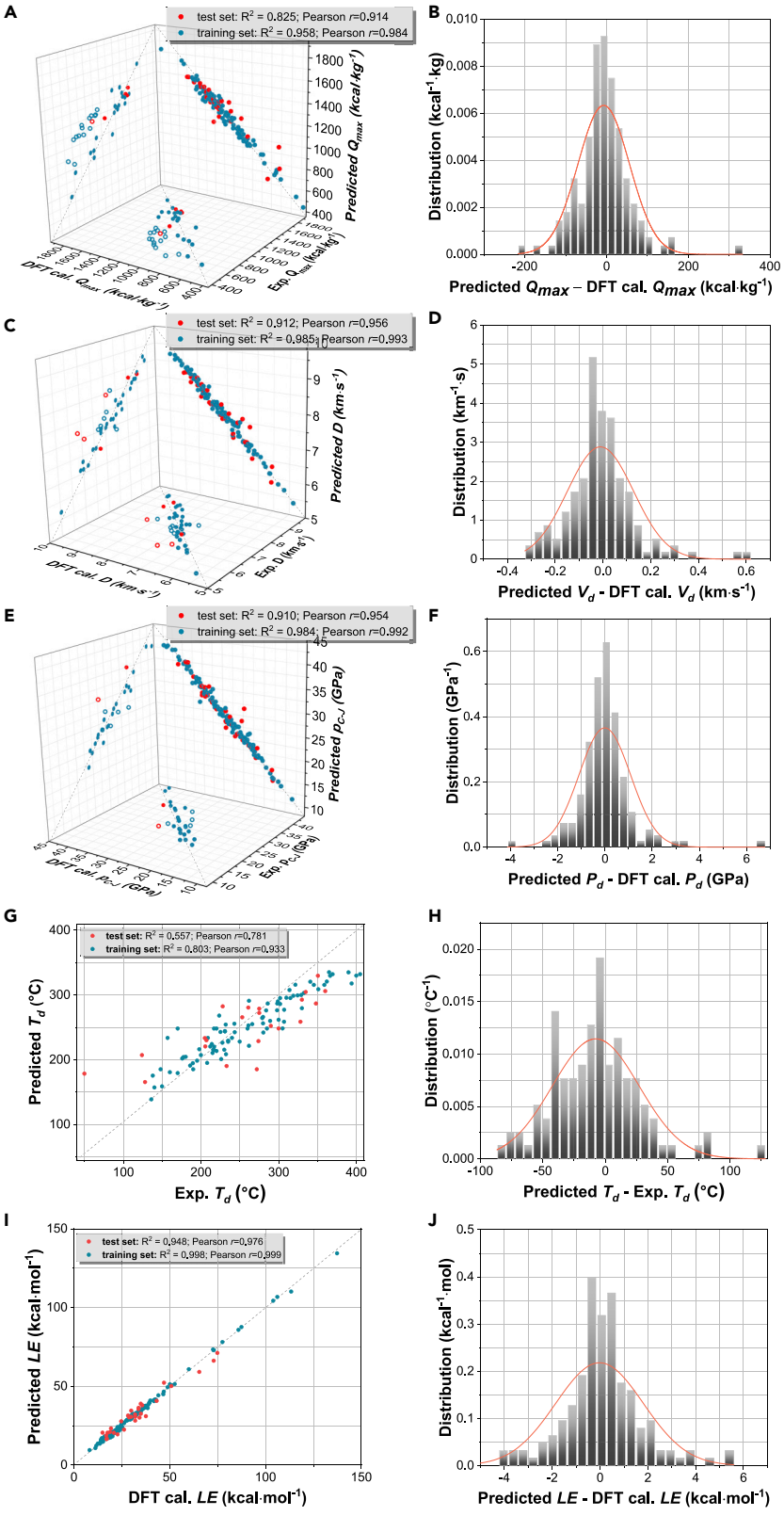
A
test set: R² = 0.825; Pearson r=0.914
training set: R² = 0.958; Pearson r=0.984
Predicted Qmax (kcal·kg⁻¹)
DFT cal. Qmax (kcal·kg⁻¹)
Exp. Qmax (kcal·kg⁻¹)
B
Distribution (kcal⁻¹·kg)
Predicted Qmax – DFT cal. Qmax (kcal·kg⁻¹)
C
test set: R² = 0.912; Pearson r=0.956
training set: R² = 0.985; Pearson r=0.993
Predicted D (km·s⁻¹)
DFT cal. D (km·s⁻¹)
Exp. D (km·s⁻¹)
D
Distribution (km⁻¹·s)
Predicted Vd - DFT cal. Vd (km·s⁻¹)
E
test set: R² = 0.910; Pearson r=0.954
training set: R² = 0.984; Pearson r=0.992
Predicted pC-J (GPa)
DFT cal. pC-J (GPa)
Exp. pC-J (GPa)
F
Distribution (GPa⁻¹)
Predicted Pd - DFT cal. Pd (GPa)
G
test set: R² = 0.557; Pearson r=0.781
training set: R² = 0.803; Pearson r=0.933
Predicted Td (°C)
Exp. Td (°C)
H
Distribution (°C⁻¹)
Predicted Td - Exp. Td (°C)
I
test set: R² = 0.948; Pearson r=0.976
training set: R² = 0.998; Pearson r=0.999
Predicted LE (kcal·mol⁻¹)
DFT cal. LE (kcal·mol⁻¹)
J
Distribution (kcal⁻¹·mol)
Predicted LE - DFT cal. LE (kcal·mol⁻¹)

Figure 4. Performance of XGBoost model in predictions of detonation and stability properties of HEDMs as well as experimental validation

(A–J) (A) Predicted values of Q_{max}, error metrics, and experimental validation. (B) Distribution of Q_{max} residuals between XGBoost prediction and DFT calculation. (C) Predicted values of D, error metrics, and experimental validation. (D) Distribution of D residuals between XGBoost prediction and DFT calculation. (E) Predicted values of $p_{C\text{-}J}$, error metrics, and experimental validation. (F) Distribution of $p_{C\text{-}J}$ residuals between XGBoost prediction and DFT calculation. (G) Predicted values of T_d and their error metrics. (H) Distribution of residuals between XGBoost prediction and experimental measurement. (I) Predicted values of LE and their error metrics. (J) Distribution of residuals between XGBoost prediction and DFT calculation. Solid spheres of experimental data are for the densely pressed samples with $\rho \geq 95\%\ \rho_{max}$, and the open circles are for those compounds with $\rho < 95\%\ \rho_{max}$. Residuals of all XGBoost predictions are shown in Figure S1.

presented in Table 1. Among the five models studied (Figures S6–S9), XGBoost model reproduced the best agreement with DFT calculations for both the training set and the test set. The scoring metrics for the training set are $RMSE = 0.10\ km \cdot s^{-1}$, $r = 0.99$, and $R^2 = 0.99$, and those for the test set are $RMSE = 0.23\ km \cdot s^{-1}$, $r = 0.96$, and $R^2 = 0.91$. Figure 4C shows an accurate prediction of D by using XGBoost model, wherein 98% of the predicted values have a relative error of <5% with respect to the DFT calculations and 100% of the predicted values have a relative error of <10%. Figure 4D presents a distribution of the residuals of the XGBoost predictions, which satisfactorily follows normal distributions. The currently obtained value of r is comparable to a previous ANN prediction of D for 65 explosive compounds and compositions, wherein, $r = 0.978$ for training set and 0.985 for test set (Chandrasekaran et al., 2019). The currently obtained values of R^2 and $RMSE$ are close to another prediction of 54 nitrogen-rich energetic compounds obtained by least square support vector machine (LS-SVM) method, in which $RMSE = 0.17\ km \cdot s^{-1}$, $r = 0.96$ for the training set and $RMSE = 0.17\ km \cdot s^{-1}$, $r = 0.97$ for the test set (Wang et al., 2014). Our metrics are overall better than those of the previous studies as follows: the decision tree boost predictions of D for 106 ideal explosives and 231 non-ideal explosives ($RMSE = 0.41\ km \cdot s^{-1}$, $r = 0.94$ for training set and $RMSE = 0.34\ km \cdot s^{-1}$, $r = 0.93$ for test set) (Gupta et al., 2016); the partial least squares regression (PLSR) predictions of D for 92 ideal, 84 non-ideal, and 68 non-explosive chemicals ($RMSE = 0.74\ km \cdot s^{-1}$, $r = 0.87$ for training set and $RMSE = 0.28\ km \cdot s^{-1}$, $r = 0.96$ for test set) (Gupta et al., 2015); the neural network (NN) predictions of D for 416 molecules ($RMSE = 0.27\ km \cdot s^{-1}$, $r = 0.86$, $R^2 = 0.93$ for test set) (Barnes et al., 2018); and the KRR predictions of D for 109 HEDMs ($r = 0.94$ and $R^2 = 0.89$ for the training set and $r = 0.91$ and $RMSE = 0.25\ km \cdot s^{-1}$, $r = 0.91$, $R^2 = 0.82$ for the test set) (Elton et al., 2018).

For the prediction of $p_{C\text{-}J}$, XGBoost model exhibited the best performance among the five models studied herein (Figures S10–S13, Supplemental information), with $RMSE$ being the lowest and r and R^2 being closest to 1. The scoring metrics are $RMSE = 0.82$ GPa, $r = 0.99$, and $R^2 = 0.98$ for the training set and $RMSE = 1.79$ GPa, $r = 0.95$, and $R^2 = 0.91$ for the test set. Figure 4E illustrates the accuracy of the XGBoost prediction of $p_{C\text{-}J}$, wherein 88.2% of the predicted values showed a relative error of <5% referring to the DFT calculation and 97.4% of the predicted values were within a relative error of <10%. Figure 4D demonstrates that the distribution of the residuals of XGBoost prediction approximately follows normal distributions. Our scores are overall more satisfactory than those achieved in the previous studies, such as the PLSR and logistic regression predictions of $p_{C\text{-}J}$ for 92 ideal, 84 non-ideal, and 68 non-explosive compounds (the best scores being $RMSE = 5.45$ GPa, $r = 0.85$ for training set and $RMSE = 2.53$ GPa, $r = 0.93$ for test set) (Gupta et al., 2015); the NN predictions of $p_{C\text{-}J}$ for 416 energetic molecules ($RMSE = 2.15$ GPa, $r = 0.93$, $R^2 = 0.87$ for test set) (Barnes et al., 2018); and the KRR predictions of $p_{C\text{-}J}$ for 109 HEDMs ($r = 0.67$ for the test set) (Elton et al., 2018).

To validate the predictions of the detonation parameters, we searched 112 experimental detonation parameters from comprehensive literature survey, but we only compared our predicted values with corresponding experimental values measured for the compounds close to its theoretical maximum density: $\rho \geq 95\%\ \rho_{max}$, wherein ρ_{max} is the maximum theoretical density as determined by X-ray crystallography. Figures 4A–4E and Table S3 (supplemental information) present satisfactory agreement between the XGBoost predictions and 83 experimental data reported for densely pressed samples with $\rho \geq 95\%\ \rho_{max}$, as marked in solid. Another 29 experimental data of the loosely pressed samples of HEDMs ($\rho < 95\%\ \rho_{max}$) are also presented in Figure 4, as marked in open circles. As expected, our XGBoost predictions (for compounds with $\rho = \rho_{max}$) are generally higher than the corresponding experimental measurements (for samples with $\rho < 95\%\ \rho_{max}$). Thus the XGBoost models in predictions of Q_{max}, D, and $p_{C\text{-}J}$ were validated.

Molecular stability characterized by decomposition temperature. The decomposition temperature (T_d) herein refers to on-set temperature of the exothermic curve, and it is employed to represent the critical temperature at which the molecule starts to lose its stability.

For the prediction of molecular stability characterized by T_d, all five models studied showed relatively poor performance compared with the predictions of detonation properties Among the five models, RF exhibited the best performance for the training set (*RMSE* = 21.23°C, r = 0.97, and R^2 = 0.90), whereas XGBoost (*RMSE* = 52.07°C, r = 0.78, and R^2 = 0.56) was the best performing model for the test set, as presented in Table 1. The distribution of residuals between XGBoost prediction and experimental measurement was close to normal distribution, as shown in Figures 4H and S14–S17. Figure 4G presents that 57.8% of the XGBoost predictions of T_d have a relative error of <10% with respect of the experimental results and 90.8% of the predictions were found to be in the range of a relative error of below 20%. A previous ANN prediction of T_d of energetic co-crystals showed high metrics with R^2 = 0.98. However, this prediction was based on a limited dataset (19 training data and 6 test data), which is too small to deliver convincing statistics (Fathollahi and Sajady, 2018). Similarly poor performance was also observed in the prediction of experimental power conversion efficiency of organic solar cell devices, where RF was identified to be the best performing model, yet with a low r value of 0.70 (Wu et al., 2020).

The quality of the T_d dataset is the fundamental reason for the relatively low performance of the current prediction of T_d and the linearity problem between residual and target data of the trained models (Figure S1D). Among the 153 HEDMs studied in this work, only 109 were found in the literature to have reported T_d. These collected T_d values from the literature search were measured using different techniques, using different parameters, and by different investigators. Among the 109 T_d values, 85 were recorded by the on-set temperature of differential scanning calorimetry (DSC) method, 9 were determined by the on-set temperature of differential thermal analysis method, and for the remaining 15 compounds, the T_d values were reported, but the measuring methods were not provided. Besides the application of various techniques, the used heating rate, sample weight, carrier gas flow rate, and other parameters were quite dispersed, all significantly affecting the results and leading to deviations in the reported T_d. For example, the different heating rate can shift the location of the exothermic peak in DSC thermograms by up to 49°C and different compositions may change the T_d of TNT by up to 73°C (Li et al., 2019). For each of the 109 T_d used, the corresponding measuring method (if known) is listed in Table S3 (Supplemental information).

The current study indicates that a unified standard for thermal analysis of HEDMs is strongly needed, and this will help experimenters generate more transferable and more reliable T_d values. Then, scientists will have more transferable and more reliable values to evaluate the molecular stability of various HEDMs. Also, ML prediction of T_d of HEDMs is expected to have much-improved performance.

Crystal stability characterized by lattice energy. For the prediction of crystal stability characterized by *LE*, XGBoost model exhibited the best performance among the five models studied (Figures S18–S21; Supplemental information). The scoring metrics are *RMSE* = 1.03 kcal·mol^{-1}, r = 1.00, and R^2 = 1.00 for the training set, and *RMSE* = 3.49 kcal·mol^{-1}, r = 0.98, and R^2 = 0.95 for the test set. Figure 4I shows a high-level reproduction of the DFT calculation of *LE*, wherein 69.3% of the XGBoost predicted values showed a relative error of <5% and 87.6% of the predicted values were within a relative error of <10%. Figure 4J indicates that the distribution of the XGBoost prediction residuals approximately follows normal distributions.

Physics insight from machine learning

Main features in determining detonation performance, molecular stability, and crystal stability

After the training and evaluation of the five models used in the prediction of D, $p_{C\text{-}J}$, Q_{max}, T_d, and *LE*, the best performing XGBoost model was eventually selected for each property to conduct feature importance analysis. In this work, the gain-type algorithm in XGBoost regression was utilized to rank feature importance. The features leading to higher average gain values in decision trees are considered more important. The resulting importance was characterized by percentage, and the rankings of the importance of the features in determining the detonation and stability properties are shown in Figure 5. Another feature importance ranking, which is quantified based on the magnitude of Pearson correlation coefficients, is presented in Table S4 (Supplemental information) for comparative analysis, although the latter method is mostly sensitive to linear dependencies.

Feature importance ranking in XGBoost predictions of heat of explosion, detonation velocity, and detonation pressure. Detonation performance, which is usually characterized by Q_{max}, D, and $p_{C\text{-}J}$, is

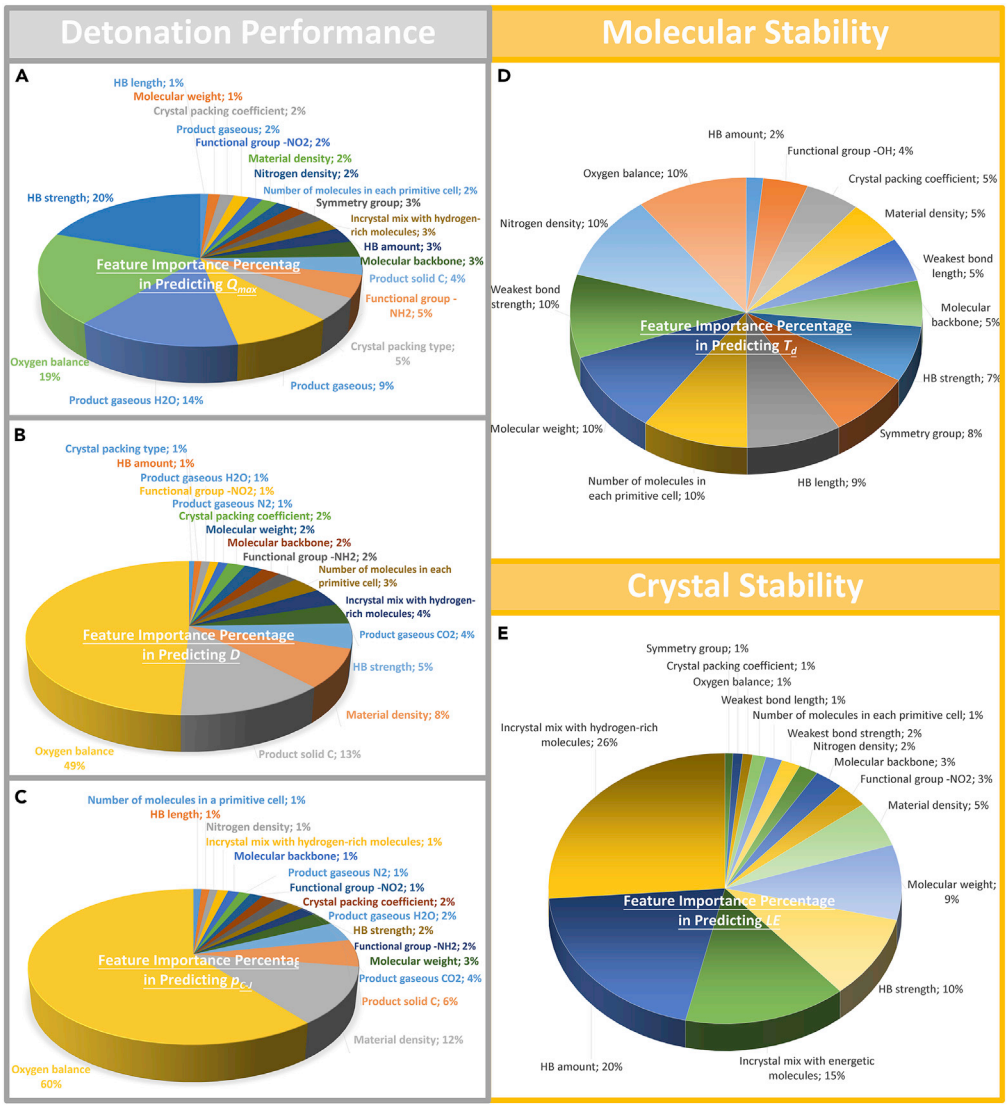

Figure 5. Pie chart of importance ranking of feature descriptors in predictions of detonation and stability properties of HEDMs

(A) Q_{max}; (B) D; (C) p_{C-J}; (D) T_d; and (E) LE.

one the most valued properties in an HEDM evaluation. Figures 5A–5C present the importance ranking of feature descriptors in the determination of detonation properties of HEDMs.

The common characteristic of the top five important features in predictions of Q_{max}, D, and p_{C-J}, are OB and the presence of gaseous CO_2 in the reaction products. Figure 5 illustrates that OB ranks as the most important feature to predict p_{C-J} and D and as the second important feature to determine Q_{max}, acquiring 60%, 49%, and 19% in the feature importance pie chart in determining p_{C-J}, D, and Q_{max}, respectively. Currently the obtained data-driven conclusion is well consistent with known professional knowledge, that is, OB describes the extent to which a certain HEDM could be oxidized and significantly affects the amount of energy released during the detonation (Figure S22; supplemental information). Figure 5 shows that the presence of gaseous CO_2 in the reaction products plays as the fourth importance role in predicting Q_{max} and p_{C-J}, and as the fifth most important parameter in predicting D, achieving 9%, 4%, and 4% of the importance percentage, respectively. Pearson correlation coefficients listed in Table S4 indicate that the presence of gaseous N_2 in the reaction products is also important to detonation properties. These results are consistent with our recent knowledge-driven

findings (Li et al., 2020a, 2020b, 2020c) that the generation of large amount of CO_2 and N_2 gas is conducive to the improvement of Q_{max}, D, and $p_{C\text{-}J}$ of HEDMs. Furthermore, it was found that molecules, with high MW value and energetic rings connected via bridge bonds or with non-planer heterocyclic or cage-like backbones, are responsible for the better Q_{max} of these molecules, whereas they have only a minimal influence on D and $p_{C\text{-}J}$ (Figure S27; Supplemental information).

In particular, the presence of gaseous H_2O in the products ranked third in determining Q_{max}; the presence of solid C ranked second in determining D and ranked third to predict $p_{C\text{-}J}$, as presented in Figure 5. Pearson correlation coefficients presented in Table S4 (Supplemental information) indicate that the contribution of the presence of gaseous H_2O in the products is negative for obtaining large value of Q_{max}, and the contribution of the presence of solid C in the products has also negative effect on obtaining large values of D and $p_{C\text{-}J}$. These results are consistent with the recent finding (Li et al., 2020a, 2020b, 2020c) that high proportion of H_2O in the products leads to a lower Q_{max} and high content of solid carbon clusters in the detonation products, which are obtained due to the oxygen deficiency in the structure of an HEDM, leads to a drastic decrease in D and $p_{C\text{-}J}$ of HEDMs.

Noteworthy, crystal features, such as the highest strength of intermolecular HB, the material density ρ, and the HB amount (characterized by the area of HB on the Hirshfeld surface of each individual molecule), are crucial for the determination of the detonation properties. Previous research noticed the importance of ρ parameter in the prediction of the detonation properties, whereas the other two features were often overlooked. HB amount and HB strength determine the interspecies association distribution, interaction strength, packing compactness, and energy level of the compound, and are therefore important to the energy that could be released in detonation. Both high HB amount and high HB strength of an HEDM could lead to a significant reduction in its detonation performance (Figures S23 and S24; Supplemental information), consistent with the negative Pearson correlation coefficients listed in Table S4 (Supplemental information). Based on our current study, the importance of crystal characteristics to detonation properties of HEDMs needs to be re-understood comprehensively.

Feature importance ranking in XGBoost prediction of molecular stability. Higher thermal stabilities usually result in HEDMs with lower sensitivities, which are safer to handle. T_d is an important characterization index of thermal stability of compounds at the molecular level, and a search for high-performance thermostable HEDMs, with T_d higher than that of hexanitrostilbene (HNS), i.e., $T_d > 330°C$, is an active research topic in the field of HEDMs (Rieckmann et al., 2001; Klapötke, 2015).

Figure 5D exhibits the description of the importance ranking of feature descriptors used for the determination of T_d. In contrast to the detonation properties, the importance percentage toward determination of T_d is rather uniform and disperse. Each of the 12 features occupies >5% of the importance percentage. These features are OB, ρ_N, the weakest/longest intramolecular bond strength/length, MW, molecular backbone, the strongest/shortest intermolecular HB strength/length, number of molecules located in each primitive cell, and symmetry group. Among them, the molecular features are more important than the crystal features.

At the molecular level, OB is important in determining T_d, i.e., higher OB results in lower T_d, which contradicts the requirement of high detonation performance (Table S4 and Figure S22; Supplemental information). Second, the weakest intramolecular bond is the trigger of the decomposition of HEDMs and plays a crucial role to determine T_d (Table S4 and Figure S26; supplemental information). Third, current result indicates that large MW and bridged or non-planar molecular backbone significantly improve T_d, in a way similar to the improvement of Q_{max} (Table S4 and Figure S27; supplemental information).

At the crystal level, HB amount and HB strength have been proved to be important in predicting T_d, as shown in Figure 5D and Table S4 (supplemental information). These features determine the crystal packing force, which in turn influences the activation energy of the molecule decomposition. Figures S23 and S24 (Supplemental information) exhibit that the requirement of high HB amount and high HB strength for high T_d contradicts the high detonation performance.

Feature importance ranking in XGBoost prediction of crystal stability. Crystal stability of HEDMs refers to the extent to which the crystals can sustain cohesion as solids against sublimation into separate

molecules. Herein, *LE* was employed to characterize crystal stability, which is defined as the total energy difference between the constituent ions in the free state and the crystal form. A comparable measurement of *LE* from experiment is the sublimation temperature. However, the reported data for the sublimation of HEDMs were extremely limited, because many of the HEDMs would not sublime but would melt. Therefore, we used melting point as an alternative value to compare with *LE*, validating the roughly positive correlation between *LE* and crystal stability, as shown in Figure S1 (supplemental information).

Figure 5E presents the importance ranking of feature descriptors in determining *LE*. In contrast to T_d, the crystal features to determine *LE* are more important than the molecular features, which is consistent with the ranking from Pearson correlation coefficients listed in Table S4 (Supplemental information). Among them, HB=relevant features are the most important to determine *LE*. The in-crystal mixing with hydrogen-rich molecules, HB amount, and HB strength together contribute 56% of the feature importance percentage. Having a higher HB amount and higher HB strength is advantageous to improve *LE*, enabling corresponding HEDMs to achieve higher thermal stability. However, they contradict with the requirement of high detonation performance (Figures S23 and S24; supplemental information).

Third ranked feature is the in-crystal mixing with of energetic molecules, which takes 15% of the importance percentage. The importance of this feature to determine *LE* confirms the rationality of co-crystallization strategy in the promotion of thermostability of HEDMs.

From the perspective of molecular level features, MW and molecular backbone are important in determining *LE*. HEDMs composed of bridged molecules with high MW are very likely to show higher *LE*. For example, the compounds such as 3,5-dinitro-*N*,*N*′-bis(2,4,6-trinitrophenyl)pyridine-2,6-diamine, 5,5′-ethane-1,2-diylbis(1H-tetrazole), and 3,3′-(1,4-phenylenediethene-2,1-diyl)bis-(2,4,6-trinitroaniline)-*N*,*N*-dimethylformamide solvate, with their energetic rings connected with $NH/NH_2/CH/CH_2$ bridge bonds, all have relatively high *LE*. 3,5-Dinitro-*N*,*N*′-bis(2,4,6-trinitro-phenyl)pyridine-2,6-diamine (MW = 621.35), constituted by three energetic rings and two "–NH–" bridges, has a high *LE* = 51.01 kcal·mol^{-1} that is 2.4 times higher than that of TNT (single energetic ring, MW = 227.20). Similarly, the compounds with non-planar heterocyclic or cage-like backbones, such as HMX (MW = 296.2) and CL-20 (MW = 438.2), have high *LE* values that are 1.8 and 1.4 times larger than that of TNT.

Guidelines for balancing performance and stability

From feature importance ranking and data statistics, herein, the features were classified into the two distinctive types: (1) contradictory features and (2) non-contradictory features, to balance the detonation performance and stability of HEDMs. Optimal ranges of all found critical features of HEDMs for balancing detonation performance and stability are presented in Table 2.

In our opinion, the OB, HB amount, and HB strength are the main parameters that lead to the performance-stability contradiction of HEDMs (Figures S22–S24; supplemental information). OB = 0% ranks first among all other features in providing the best $p_{C\text{-}J}$ and *D* values, whereas it also ranks first in reducing T_d. Considering the detonation properties ($p_{C\text{-}J}$ = 22.35 GPa and *D* = 7.15 km·s^{-1}) and detonation temperature (T_d = 225°C) of TNT, as a reference, the optimal range of OB that balances detonation and stability is in the range of −60% < OB < 0%. HB amount seems to be the most significant feature that causes detonation performance-crystal stability contradiction. Abundant HB is the most important requirement of high *LE*; however, high amount of HBs is accompanied with a high proportion of H_2O in the detonation products, thereby decreasing Q_{max}. Figure S23 (supplemental information) illustrates that there is no intersection of HB amount to simultaneously satisfy high detonation performance and high crystal stability. However, if application of the designed HEDM mostly demands high $p_{C\text{-}J}$ and *D*, regardless of Q_{max}, the optimal range of HB amount can be >90 Å^2. In case that a high T_d of the designed HEDM is the main objective, whereas high crystal stability is less important, the optimal range for such HEDMs could be further extended to be HB amount >30 Å^2. High HB strength leads to a reduced total energy of the system, thereby decreasing Q_{max} of HEDMs. However, high HB strength is important for HEDMs to reach high *LE* and high T_d. To balance detonation performance and crystal stability, the recommended range of the strength of the strongest HB is in the range of 2.5 < HB σ < 5.0 kcal·mol^{-1}. However, HB strength has a limited relevance to $p_{C\text{-}J}$ and *D*. If application of the designed HEDM mostly demands high *D* and $p_{C\text{-}J}$, regardless of Q_{max}, the optimal range of HB strength is recommended to be HB amount >2.5 kcal·mol^{-1}.

Table 2. Optimal ranges of critical features of HEDMs for balancing detonation performance and stability

Features	Optimal ranges
Oxygen balance (OB)	$-60 < OB < 0\%$
HB strength σ	HB $\sigma > 2.5$ kcal mol^{-1}
	$2.5 <$ HB $\sigma < 5.0$ kcal mol^{-1} (regardless Q_{max})
HB amount	Ø
	>90 Å^2 (regardless Q_{max})
	>30 Å^2 (regardless Q_{max} and *LE*)
Material density (ρ)	$\rho > 1.73$ g cm^{-3}
Weakest intramolecular strength (σ)	$\sigma > 70.0$ kcal mol^{-1}
Molecular weight	>250 Da
Molecular backbone	Bridged backbones
	Non-planar backbones of heterocycles or cages

In this work, it was found that ρ and the weakest intramolecular bonds are non-contradictory features in balancing detonation performance and crystal stability. Although a high ρ is always a pursuit for achieving high detonation performance of HEDMs, it has little relevance to T_d or *LE* (Figure S25; supplemental information). Considering the detonation performance of TNT as a reference, the recommended range is $\rho > 1.73$ g·cm^{-3}. Strong intramolecular bonds and high MW are important for HEDMs to improve both molecular stability and crystal stability. Theoretically, stronger bond decreases the energy level of energetic molecules, leading to a small energy difference between the reactants and the products, and thereby reduction in the detonation performance of HEDMs. Yet, feature importance analysis shows that the strength of intra-molecular bonds does not significantly influence detonation properties. Therefore, strengthening the intramolecular bonds can be a potential way to balance the detonation and stability of HEDMs, and the recommended range is $\sigma > 70.0$ kcal mol^{-1} (Figure S26; supplemental information).

Very importantly, it was found that the design of molecules with high MW, bridged backbones, or non-planar heterocyclic or cage-like backbones could lead to simultaneous improvement in the detonation performance and the stability of HEDMs. Furthermore, co-crystallization is an effective strategy for improving the thermal stability of HEDMs.

DISCUSSION

In this study, ML methodology was employed to better understand intricate causality of the detonation performance-stability contradiction, and to facilitate more efficient rational design of advanced HEDMs, by providing data-driven recommendations of critical parameters. More specifically, quantum mechanics method was used to calculate 21,648 physicochemical parameters, detonation properties, and stability properties of 153 reported HEDMs, which were then used as the input for training of five ML models, i.e., XGBoost, AdaBoost, RF, MLP, and KRR. Stratified sampling was employed to classify training set and test set by a ratio of 4:1, and grid search and cross-validation loop were conducted for more than 12,500 times in total to optimize the hyper-parameters in predicting D, $p_{C\text{-}J}$, Q_{max}, T_d, and *LE* of the HEDMs. By evaluating the scoring metrics, the distribution of prediction residuals, and the deviation from experimental data, XGBoost model was proved to exhibit the best performance in predictions of all five properties of HEDMs.

Furthermore, feature importance analysis was carried out by two methods, i.e., the gain-type algorithm in XGBoost regression and the magnitude of Pearson correlation coefficients. The contradictory features and non-contradictory features in balancing detonation performance and stability of HEDMs were subsequently screened out. The optimal range of key features, which facilitated the optimal balance between the two contradictory factors, was identified to be (1) $-60 < OB < 0\%$, (2) HB strength >2.5 kcal·mol^{-1}, (3) $\rho > 1.73$ g·cm^{-3}, (4) the weakest intramolecular strength >70.0 kcal·mol^{-1}, (5) and MW > 250 Da. Design of molecules with large MW, bridged backbones, and non-planar backbones of heterocycles or cages, are generally favorable in improving both detonation performance and stability of HEDMs.

Limitations of the study

There is a linearity problem between residual data and target data in the prediction of decomposition temperature T_d. We tried several methods to fix this problem, for example, adjusting model parameters, using standardized fingerprints, and using Box-Cox transformation for target data. However, all these attempts failed. We later tried to artificially modify the trained models according to the fitted linear relation between the predicted data and the target data of the training set. Although the linearity problem in XGBoost, AdaBoost, and RF models was finally fixed, artificial fixing of the trained model may confuse the readers and cause misleading. We finally decided to respect the truth and use the originally trained model, instead of the artificially fixed ones.

As we have discussed in the section molecular stability characterized by decomposition temperature, the T_d dataset was searched from massive literature. The quality of the T_d dataset is the fundamental reason that various models cannot learn T_d, leading to the linearity problem and the low scoring metrics in predicting T_d. The current study indicates that a unified standard for thermal analysis of HEDMs is strongly needed, and this will help experimenters generate more transferable and more reliable T_d values. Then, scientists will have more reliable values to evaluate the stability of various HEDMs. Also, ML on the stability of HEDMs is expected to have much-improved performance.

Resource availability

Lead contact

Further information and requests for resources should be directed to the lead contact, Lei Zhang (zhang_lei@iapcm.ac.cn).

Materials availability

This study did not generate new unique reagents.

Data and code availability

The source data that support the findings of this study and the used codes are available from the corresponding authors upon reasonable request.

METHODS

All methods can be found in the accompanying transparent methods supplemental file.

SUPPLEMENTAL INFORMATION

Supplemental Information can be found online at https://doi.org/10.1016/j.isci.2021.102240.

ACKNOWLEDGMENTS

The authors greatly acknowledge the financial support from the National Natural Science Foundation of China (Grant Nos. 12072045, 11702266, 11972329, and 51703211). L. Z. thanks Prof. C. Y. Zhang, J. G. Zhang, and S. L. Huang for the helpful discussions. Y.W. thanks Q. Ma, Q. Zeng, and R. Liu for the helpful discussions.

AUTHOR CONTRIBUTIONS

X.H. and F.G. debugged machine learning codes and performed training and evaluation of five machine learning models. C.L. performed DFT calculations and collected experimental data from extensive literature search. K.T., M.L., Y.H., C.Q.S., and M.G. jointly discussed and co-wrote the manuscript. Y.W. guided the use of machine learning techniques in high energy density materials and co-wrote the manuscript. L.Z. conceived the theory, designed the calculations, and drafted the manuscript. All authors contributed to the overall scientific interpretation.

DECLARATION OF INTERESTS

The authors declare no competing interests.

Received: November 6, 2020
Revised: January 17, 2021
Accepted: February 23, 2021
Published: March 19, 2021

REFERENCES

Agrawal, J.P. (2010). High Energy Materials-Propellants, Explosives and Pyrotechnics (WILEY-VCH Verlag GmbH & Co. KGaA).

Barnes, B.C., Elton, D.C., Boukouvalas, Z., Taylor, D.E., Mattson, W.D., Fuge, M.D., and Chung, P.W. (2018). Machine learning of energetic material properties. arXiv, 1807.06156.

Barnes, B., Rice, B., and Sifain, A. (2020). Machine learning of energetic material properties and performance. Bull. Am. Phys. Soc. *65*, G20.00009.

Butler, K.T., Davies, D.W., Cartwright, H., Isayev, O., and Walsh, A. (2018). Machine learning for molecular and materials science. Nature *559*, 547–555.

Chandrasekaran, N., Oommen, C., Kumar, V.R.S., Lukin, A.N., Abrukov, V.S., and Anufrieva, D.A. (2019). Prediction of detonation velocity and N−O composition of high energy C−H−N−O explosives by means of artificial neural networks. Propellants Explos. Pyrotech. *44*, 579–587.

Cho, S.G., No, K.T., Goh, E.M., Kim, J.K., Shin, J.H., Joo, Y.D., and Seong, S. (2005). Optimization of neural networks architecture for impact sensitivity of energetic molecules. Bull. Korean Chem. Soc. *26*, 399–408.

Elton, D.C., Boukouvalas, Z., Butrico, M.S., Fuge, M.D., and Chung, P.W. (2018). Applying machine learning techniques to predict the properties of energetic materials. Sci. Rep. *8*, 1–12.

Fathollahi, M., and Sajady, H. (2018). QSPR modeling of decomposition temperature of energetic cocrystals using artificial neural network. J. Therm. Anal. Calorim. *133*, 1663–1672.

Granda, J.M., Donina, L., Dragone, V., Long, D.-L., and Cronin, L. (2018). Controlling an organic synthesis robot with machine learning to search for new reactivity. Nature *559*, 377–381.

Gupta, S., Basant, N., and Singh, K.P. (2015). Identifying high energy molecules and predicting their detonation potency using chemometric modelling approaches. Combust. Theor. Modell. *19*, 451–464.

Gupta, S., Basant, N., and Singh, K.P. (2016). Three-tier strategy for screening high-energy molecules using structure–property relationship modeling approaches. Ind. Eng. Chem. Res. *55*, 820–831.

He, H., Zhang, L., Wei, B., Sheng, L., Yi, Y., and Jun, C. (2017). Structural, mechanical properties and vibrational spectra of LLM-105 under high pressures from a first-principles study. J. Mol. Model. *23*, 275.

Hu, L., Gao, H., and Shreeve, J.N. (2020). Challenging the limits of nitrogen and oxygen content of fused rings. J. Mater. Chem. A *8*, 17411–17414.

Jiang, C., Zhang, L., Sun, C., Zhang, C., Yang, C., Chen, J., and Hu, B. (2018). Response to comment on "Synthesis and characterization of the pentazolate anion *cyclo*-N_5^- in $(N_5)_6(H_3O)_3(NH_4)_4Cl$.". Science *359*, eaas8953.

Jiao, F., Xiong, Y., Li, H., and Zhang, C. (2018). Alleviating the energy & safety contradiction to construct new low sensitive and high energetic materials through crystal engineering. CrystEngComm *20*, 1757–1768.

Kang, P., Liu, Z., Abou-Rachid, H., and Guo, H. (2020). Machine-learning assisted screening of energetic materials. J. Phys. Chem. A *124*, 5341–5351.

Klapötke, T.M. (2015). Chemistry of High-Energy Materials (Walter de Gruyter GmbH & Co KG).

Lang, Q., Sun, Q., Wang, Q., Lin, Q., and Lu, M. (2020). Embellishing bis-1,2,4-triazole with four nitroamino groups: advanced high-energy-density materials with remarkable performance and good stability. J. Mater. Chem. A *8*, 11752–11760.

Li, C., Huang, Y., Sun, C.Q., and Zhang, L. (2020a). Theoretical study on improvement strategy of crystal stability and detonation energy of cocrystal explosive. Chin. J. Energ. Mater. *28*, 854–860.

Li, C., Li, H., Zong, H.-H., Huang, Y., Gozin, M., Sun, C.Q., and Zhang, L. (2020b). Strategies for achieving balance between detonation performance and crystal stability of high energy density materials. iScience *23*, 100944.

Li, H., Zhang, L., Petrutik, N., Wang, K., Ma, Q., Shem-Tov, D., Zhao, F., and Gozin, M. (2020c). Molecular and crystal features of thermostable energetic materials: guidelines for architecture of "bridged" compounds. ACS Cent. Sci. *6*, 54–75.

Li, J.-S., Chen, J.-J., Hwang, C.-C., Lu, K.-T., and Yeh, T.-F. (2019). Study on thermal characteristics of TNT based melt-cast explosives. Propellants Explos. Pyrotech. *44*, 1270–1281.

Lu, S., Zhou, Q., Ouyang, Y., Guo, Y., Li, Q., and Wang, J. (2018). Accelerated discovery of stable lead-free hybrid organic-inorganic perovskites via machine learning. Nat. Commun. *9*, 3405.

Mancuso, J.L., Mroz, A.M., Le, K.N., and Hendon, C.H. (2020). Electronic structure modeling of metal–organic frameworks. Chem. Rev. *120*, 8641–8715.

Mo, Z., Zhang, A., Cao, X., Liu, Q., Xu, X., An, H., Pei, W., and Zhu, S. (2010). JASMIN: a parallel software infrastructure for scientific computing. Front. Comput. Sci. China *4*, 480–488.

Nefati, H., Cense, J.-M., and Legendre, J.-J. (1996). Prediction of the impact sensitivity by neural networks. J. Chem. Inf. Comput. Sci. *36*, 804–810.

Rieckmann, T., Völker, S., Lichtblau, L., and Schirra, R. (2001). Investigation on the thermal stability of hexanitrostilbene by thermal analysis and multivariate regression. Chem. Eng. Sci. *56*, 1327–1335.

Rupeng, B., Xiong, Y., Wei, X., Li, H., and Zhang, C. (2019). Hydrogen bonding in CHON contained energetic crystals: a review. Cryst. Growth Des. *19*, 5981–5997.

Sabin, J.R. (2014). Advances in Quantum Chemistry (Academic Press).

Sanchez-Lengeling, B., and Aspuru-Guzik, A. (2018). Inverse molecular design using machine learning: Generative models for matter engineering. Science *361*, 360.

Shi, B., and Iyengar, S.S. (2020). Mathematical Theories of Machine Learning - Theory and Applications (Springer Nature).

Shukla, M.K., Boddu, V.M., Steevens, J.A., Damavarapu, R., and Leszczynski, J. (2017). Energetic Materials: From Cradle to Grave (Springer International Publishing).

Tang, Y., Huang, W., Imler, G., Parrish, D., and Shreeve, J.N. (2020). Enforced planar FOX-7-like molecules: a strategy for thermally stable and insensitive π-conjugated energetic materials. J. Am. Chem. Soc. *142*, 7153–7160.

Tang, Y., Kumar, D., and Shreeve, J.M. (2017). Balancing excellent performance and high thermal stability in a dinitropyrazole fused 1,2,3,4-tetrazine. J. Am. Chem. Soc. *139*, 13684–13687.

Wang, D., He, G., and Chen, H. (2014). Prediction for the detonation velocity of the nitrogen-rich energetic compounds based on quantum chemistry. Russ. J. Phys. Chem. A *88*, 2363–2369.

Wang, R., Jiang, J., and Pan, Y. (2012). Prediction of impact sensitivity of nonheterocyclic nitroenergetic compounds using genetic algorithm and artificial neural network. J. Energ. Mater. *30*, 135–155.

Wang, Y., Liu, Y., Song, S., Yang, Z., Qi, X., Wang, K., Liu, Y., Zhang, Q., and Tian, Y. (2018). Accelerating the discovery of insensitive high-energy-density materials by a materials genome approach. Nat. Commun. *9*, 2444.

Wejsa, J. (2014). U.S. Army Armament Research, Development, & Engineering Center (ARDEC) Energetics. Joint Armaments Conference 2014 of Conference.

Wu, Y., Guo, J., Sun, R., and Min, J. (2020). Machine learning for accelerating the discovery of high-performance donor/acceptor pairs in non-fullerene organic solar cells. NPJ Comput. Mater. *6*, 1–8.

Xu, J., Zhu, L., Fang, D., Wang, L., Xiao, S., Liu, L., and Xu, W. (2012). QSPR studies of impact

sensitivity of nitro energetic compounds using three-dimensional descriptors. J. Mol. Graphics Modell. *36*, 10–19.

Yu, Q., Yang, H., Imler, G., Parrish, D., Cheng, G., and Shreeve, J.N. (2020). Derivatives of 3,6-Bis(3-aminofurazan-4-ylamino)-1,2,4,5-tetrazine: excellent energetic properties with lower sensitivities. ACS Appl. Mater. Interfaces *12*, 31522–31531.

Zahrt, A.F., Henle, J.J., Rose, B.T., Wang, Y., Darrow, W.T., and Denmark, S.E. (2019). Prediction of higher-selectivity catalysts by computer-driven workflow and machine learning. Science *363*, eaau5631.

Zhang, C., Xue, X., Cao, Y., Zhou, J., Zhang, A., Li, H., Zhou, Y., Xu, R., and Gao, T. (2014). Toward low-sensitive and high-energetic co-crystal II: structural, electronic and energetic features of CL-20 polymorphs and the observed CL-20-based energetic-energetic co-crystals. CrystEngComm *16*, 5905.

Zhang, J., Chen, G., and Gong, X. (2017). QSPR modeling of detonation parameters and sensitivity of some energetic materials: DFT vs. PM3 calculations. J. Mol. Model. *23*, 193.

Zhang, L., Jiang, S., Yu, Y., Long, Y., Zhao, H., Peng, L., and Chen, J. (2016a). Phase transition in octahydro-1,3,5,7-tetranitro-1,3,5,7-tetrazocine (HMX) under static compression: an application of the first-principles method specialized for CHNO solid explosives. J. Phys. Chem. B *120*, 11510–11522.

Zhang, L., Wu, J., Jiang, S., Yu, Y., and Chen, J. (2016b). From intermolecular interactions to structures and properties of a novel cocrystal explosive: a first-principles study. Phys. Chem. Chem. Phys. *18*, 26960–26969.

Zhang, L., Jiang, S.L., Yu, Y., and Chen, J. (2019a). Revealing solid properties of high-energy-density molecular cocrystals from the cooperation of hydrogen bonding and molecular polarizability. Sci. Rep. *9*, 1257.

Zhang, L., Yao, C., Yu, Y., Jiang, S., Sun, C.Q., and Chen, J. (2019b). Stabilization of the dual-aromatic *cyclo*-N_5–anion by acidic entrapment. J. Phys. Chem. Lett. *10*, 2378–2385.

Zhang, L., Yao, C., Yu, Y., Wang, X., Sun, C., and Chen, J. (2019c). Mechanism and functionality of pnictogen dual aromaticity in pentazolate crystals. ChemPhysChem *20*, 2525–2530.

Zhang, L., Yu, Y., and Xiang, M.-Z. (2019d). A study of the shock sensitivity of energetic single crystals by large-scale Ab initio molecular dynamics simulations. Nanomaterials *9*, 1251.

Zhong, M., Tran, K., Min, Y., Wang, C., Wang, Z., Dinh, C.-T., De Luna, P., Yu, Z., Rasouli, A.S., Brodersen, P., et al. (2020). Accelerated discovery of CO2 electrocatalysts using active machine learning. Nature *581*, 178–183.

Zong, H.-H., Yao, C., Sun, C.Q., Zhang, J.-G., and Zhang, L. (2020). Structure and stability of aromatic nitrogen heterocycles used in the field of energetic materials. Molecules *25*, 3232.

iScience, Volume *24*

Supplemental information

Applying machine learning to balance performance and stability of high energy density materials

Xiaona Huang, Chongyang Li, Kaiyuan Tan, Yushi Wen, Feng Guo, Ming Li, Yongli Huang, Chang Q. Sun, Michael Gozin, and Lei Zhang

Supplementary Information

Table of contents

Transparent methods

All the 21648 physicochemical parameters, detonation performance parameters and stability properties of 153 HEDMs were calculated directly on a crystal level based on the recently developed supercomputing density functional theory (DFT) software, namely, High Accuracy atomistic Simulation package for Energetic Materials (HASEM)(Zhang et al., 2016), which is adapted to modern supercomputers on the basis of the J parallel Adaptive Structured Mesh applications INfrastructure (JASMIN)(Mo et al., 2010).

The training and evaluation of XGBoost model were performed using the XGBoost package, and those of AdaBoost, RF, MLP, and KRR were performed using the scikit-learn package. Stratified sampling was employed to classify training set and test set by a ratio of 4:1. Grid search and cross-validation loop were conducted to optimize the hyperparameters in predicting detonation velocity D, detonation pressure $p_{C\text{-}J}$, heat of explosion $Q_{max,}$ decomposition temperature T_d and lattice energy LE of the HEDMs. By evaluating the soring metrics, the distribution of prediction residuals and the deviation from experimental data, the best performing model was selected for feature importance analysis.

Table S3. Collected experimental data of detonation performance (heat of explosion Q_{max}, in kcal/kg, detonation velocity D, in km/s, and detonation pressure $p_{C\text{-}J}$, in GPa), molecule stability (decomposition temperature T_d, in °C), and crystal stability (melting temperature, in °C) of the 153 HEDMs studied in this work. Solid scatters ● are for the densely pressed samples with $\rho \geq 95\%\ \rho_{max}$, and open circles ○ are for those compounds with $\rho < 95\%\ \rho_{max}$, wherein ρ_{max} is the maximum theoretical density as determined by X-ray crystallography. The value in the bracket of the T_d column is the heating rate, in °C per minute, and the thermal analysis method (if it is recorded in the original experiment) is also presented. (Related to Figure 4)

	CSD No.	CAS No.	Detonation performance			Molecule stability		Crystal stability
			Q_{max}	D	$p_{C\text{-}J}$	T_d	method	Melting temperature
1	SEDTUQ	145250-81-3	--	--	--	230.85(Crawford et al., 2007)	DSC	238(decomp)(Cai et al., 2004)
2	NOETNA02	19836-28-3	1248(●)(Meyer et al., 2007)	8.85(●)(Tsyshevsky et al., 2017)	35.5(●)(Dong et al., 1989)	177.4(Liu et al., 2016)	DSC	93.5(Liu et al., 2016)
3	TATNBZ	3058-38-6	935(●)(Akst, 1989)	7.76(●)(Keshavarz, 2008)	26.8(●)(Wang et al., 2006)	366.4(Nair et al., 2007)	DSC	365(Atkins et al., 1986)
4	NTROMA01	75-52-5	1152(●)(Keshavarz, 2012)	6.35(○)(Meyer et al., 2007)	--	390(Taylor et al., 2002)	--	-28.6(Bagryanskaya et al., 1983)
5	SEDTUQ09	145250-81-3	978(●)(Meyer et al., 2007)	8.34(●)(Bemm et al., 1998)	34.0(●)(Bemm and Östmark, 1998)	--	--	--

6	SEDTUQ06	145250-81-3	--	--	--	--	--	--
7	NXENAM01	4185-47-1	1304(●)(Keshavarz, 2005)	8.00(●)(Rothstein et al., 1979)	31.0(●)(Wang et al., 2006)	189.6(10)(Zhang et al., 2018)	DSC	51.32(10)(Zhang et al., 2018)
8	NOEURA	918-99-0	1465(●)(Meyer et al., 2007)	9.00(●)(Rothstein and Petersen, 1979)	--	--	--	185(Kwasny et al., 1980)
9	NABMUY01	28464-24-6	--	8.10(●)(Tsyshevsky et al., 2017)	--	--	--	--
10	PERYTN12	78-11-5	1504(●)(Dong and Zhou, 1989)	8.60(●)(Dong and Zhou, 1989)	35.0(●)(Kamlet et al., 1968)	208(Lee et al., 2002)	DSC	142.2(Lange et al., 2009)
11	ZZZQSC02	606-20-2	795(○)(Keshavarz, 2012)	--	--	285(Lewis et al., 1996)	--	66(Bachman et al., 1958)
12	TNOXYL	632-92-8	844(○)(Keshavarz, 2005)	6.70(●)(Wang et al., 2006)	21.2(●)(Wang et al., 2006)	209(Guo et al., 2006)	DSC	182(Meyer et al., 2016)
13	DNNAPH	605-71-0	724(○)(Keshavarz, 2012)	5.52(●)(Wang et al., 2006)	--	--	--	217(Trotter, 1960)

14	GEMZAZ	55510-04-8	717(○)(Meyer et al., 2007)	7.58(○)(Dong and Zhou, 1989)	30.1(●)(Wang et al., 2006)	215(Khire et al., 2005)	DTA	249(decomp)(Boileau et al., 1985)
15	HNIABZ20	19159-68-3	1420(●)(Headqurters, 1984)	7.31(○)(Keshavarz, 2008)	--	348.1(10)(Zhang et al., 2013)	DSC	215(Leemann et al., 1908)
16	PUTCEM	25243-36-1	980(○)(Meyer et al., 2007)	7.25(●)(Keshavarz, 2008)	--	394.0(5)(Altmann et al., 1998)	--	378(Meyer et al., 2016)
17	NTRGUA03	556-88-7	653(●)(Meyer et al., 2007)	7.98(○)(Keshavarz et al., 2005)	24.5(●)(Hobbs et al., 1993)	230(Antonangeli et al., 2010)	--	232(decomp)(Davis et al., 1925)
18	DNEDAM	505-71-5	1023(●)(Meyer et al., 2007)	8.23(●)(Rothstein and Petersen, 1979)	27.3(○)(Gill et al., 2006)	180.3(Hussein et al., 2018)	DSC	178(Hall et al., 1951)
19	CORYIR	55-63-0	1485(●)(Meyer et al., 2007)	7.59(○)(Meyer et al., 2007)	25.3(○)(Hobbs and Baer, 1993)	50(Kim et al., 2018)	--	14(Altenburg et al., 2009)
20	CIWMEA10	97645-24-4	1516(●)(Keshavarz, 2012)	--	--	226(Sikder et al., 2004)	DSC	100(Singh et al., 2005)

21	QOYJOD	932-64-9	722(●)(Volk et al., 1997)	7.86(●)(Meyer et al., 2007)	31.5(○)(Akst, 1989)	279(Wu et al., 2015)	DSC	270(Schmidt et al., 1965)
22	WEKGUP	25242-76-6	1271(●)(Meyer et al., 2007)	7.77(○)(Meyer et al., 2007)	--	170.0(6)(Licht et al., 1988)	DTA	--
23	DNITBZ02	100-25-4	--	6.50(●)(Wang et al., 2006)	--	--	--	174(Boyer et al., 1959)
24	DNBENZ11	99-65-0	--	6.38(●)(Wang et al., 2006)	--	216.8(Wang et al., 2014)	DSC	90.3(McNeil et al., 2013)
25	ZZZGVU02	121-14-2	763(○)(Keshavarz, 2012)	--	--	280(Colonna et al., 2010)	--	70(Bachman and Vogt, 1958)
26	TNITAN	3698-54-2	1023(○)(Meyer et al., 2007)	--	--	216(decomp)(Dobratz et al., 1985)	--	--
27	CTMTNA03	121-82-4	1340(●)(Akst, 1989)	8.75(●)(Dong and Zhou, 1989)	34.7(●)(Politzer et al., 2011)	--	--	--
28	CTMTNA04	121-82-4	--	--	--	235(10)(Jiao et al., 2014)	DSC	206(10)(Jiao et al., 2014)

29	OCHTET	2691-41-0	--	--	--	--	--	--
30	OCHTET01	2691-41-0	1321(●)(Dong and Zhou, 1989)	9.01(●)(Politzer and Murray, 2011)	37.3(●)(Wang et al., 2006)	--	--	--
31	OCHTET03	2691-41-0	--	--	--	280.3(Gao et al., 2014)	DSC	279(Gao et al., 2014)
32	PUBMUU01	135285-90-4	--	--	--	--	--	--
33	PUBMUU07	135285-90-4	--	--	--	227.6(Gao et al., 2014)	DSC	252(decomp)(Gore et al., 2007)
34	PUBMUU12	135285-90-4	1454(●)(Meyer et al., 2007)	9.38(●)(Politzer and Murray, 2011)	44.1(●)(Keshavarz, 2008)	--	--	--
35	TNBENZ12	99-35-4	947(○)(Keshavarz, 2005)	7.30(●)(Meyer et al., 2007)	21.9(●)(Kamlet and Dickinson, 1968)	305.1(Zeman, 1980)	DTA	106(Kofler et al., 1948)
36	ZZZMUC08	118-96-7	1290(●)(Headqurters, 1984)	6.93(●)(Keshavarz, 2008)	22.5(●)(Kamlet and Dickinson, 1968)	225(10)(Hong et al., 2015)	DSC	80.8(Šarlauskas, 2010)

37	TNIOAN	489-98-5	858(○)(Keshavarz, 2007)	7.30(●)(Meyer et al., 2007)	24.7(●)(Wang et al., 2006)	324.38(20)(Zeman, 1993)	DSC	188(Spencer et al., 1946)
38	QAGBAB	96-91-3	639(○)(Keshavarz, 2007)	--	--	217(5)(Wurzenberger et al., 2020)	DTA	169.9(Meyer et al., 2016)
39	PICRAC12	88-89-1	1032(○)(Rice et al., 2002)	7.57(●)(Wang et al., 2006; Keshavarz, 2008)	27.7(●)(Wang et al., 2006)	274(10)(Hong et al., 2015)	DSC	122(Srinivasan et al., 2006)
40	SAWBUN	129-66-835860-50-5	947(○)(Keshavarz, 2005)	--	--	231(5)(Zeman, 2003)	DTA	228.7(decomp)(Fonger et al., 2014)
41	DATNBZ	1630-08-6	980(●)(Rice and Hare, 2002)	7.52(●)(Politzer and Murray, 2011)	25.9(●)(Kamlet and Dickinson, 1968)	358.96(20)(Zeman, 1993)	DSC	288(Siele et al., 1962)
42	WEKGOJ	78013-51-1	1056(○)(Keshavarz, 2007)	7.47(○)(Meyer et al., 2007)	--	300(Licht and Ritter, 1988)	DTA	162(Licht and Ritter, 1988)
43	GETFIU	4682-03-5	--	6.60(○)(Meyer et al., 2007)	--	157(5)(Fischer et al., 2016)	DSC	--

44	TNPHNT	4732-14-3	840(○)(Keshavarz, 2008)	6.50(●)(Meyer et al., 2007)	--	--	--	151(Leonard et al., 1956)
45	MTNANL01	479-45-8	1450(●)(Headqurters, 1984)	7.57(●)(Meyer et al., 2007)	26.3(●)(Kamlet and Dickinson, 1968)	170(Lee et al., 1986)	DSC	131.5(Kim et al., 2018)
46	HNIDPA	131-73-7	974(○)(Keshavarz, 2005)	7.20(○)(Meyer et al., 2007)	28.8(○)(Wang et al., 2006)	275(10)(Huang et al., 2011)	DSC	254(Huang et al., 2011)
47	GIMBOT	20062-22-0	1360(●)(Headqurters, 1984)	7.06(●)(Politzer and Murray, 2011)	26.2(●)(Headqurters, 1984)	330(2.5)(Rieckmann et al., 2001)	DSC	318(Klapötke et al., 2016)
48	BAKLII	56140-58-0	--	--	--	275(Zhang et al., 2010)	DSC	270(Blanksma, 1908)
49	DACYEL	97217-74-8	--	--	--	--	--	240(Chaykovsky et al., 1990)
50	AFEPUX	134282-42-1	--	--	--	232.0(5)(Klapötke et al., 2016)	DSC	--
51	TIBMUM	39771-28-3	--	--	--	321.6(10)(Li et al., 2003)	DSC	--
52	IKIMIY	436848-40-7	--	--	--	160.0(Averkiev et al., 2002)	--	--

53	TIBMIA	132683-64-8	--	7.9(●)(Du et al., 2013)	28.1(●)(Du et al., 2013)	350.7(10)(He et al., 2013)	DSC	--
54	YEKQAG	194486-77-6	--	7.99(●)(ZHAO et al., 2013)	29.6(●)(ZHAO and LIU, 2013)	345.3(5)(Wang et al., 2014)	DSC	--
55	CIWMAW	52173-59-8	--	--	--	302(Huang et al., 2019)	DSC	300(decomp)(Guillou et al., 2009)
56	KUBVAH	1246853-06-4	--	--	--	--	--	211(Zaitsev et al., 2009)
57	MOCJUK01	4433-16-3	--	--	--	286(Yan et al., 2019)	DSC	242.0(Roháč et al., 2008)
58	HIQBIV	131394-27-9	--	--	--	365.0(5)(Kumar et al., 2018)	DSC	305.0(Kumar et al., 2018)
59	PITGAD	2411964-98-0	--	--	--	314.0(5)(Domasevitch et al., 2019)	DTA	306.0(Domasevitch et al., 2019)
60	DORYOA	1573131-04-0	--	--	--	284(Li et al., 2014)	DSC	250(Li et al., 2014)
61	PITGEH	175788-77-9	--	--	--	298.0(5)(Domasevitch et al., 2019)	DTA	292.0(Domasevitch et al., 2019)
62	HIQBOB	1006545-77-2	--	--	--	205.5(5)(Kumar et al., 2018)	DSC	--
63	SEFVIL	2215034-55-0	--	--	--	253.2(5)(Tang et al., 2017)	DSC	209.0(Tang et al., 2017)

64	BADRAC	1605347-16-7	--	--	--	--	--	241.0(Yin et al., 2015)
65	WACGOW	32255-27-9	--	7.29(●)(Türker, 2012)	--	--	--	231.0(Terrier et al., 1990)
66	GATFEP	2072820-21-2	--	--	--	310.0(5)(Fischer et al., 2016)	DSC	--
67	GATFUF	2072820-20-1	--	--	--	205.0(5)(Fischer et al., 2016)	DSC	--
68	KIQYUH	NA	--	--	--	319.0(5)(Bölter et al., 2018)	DSC	156.0(Bölter et al., 2018)
69	KIQNUW	NA	--	--	--	330.0(5)(Bölter et al., 2018)	DSC	191.0(Bölter et al., 2018)
70	YAHKID	5180-53-0	--	--	--	332.6(Huang et al., 2011)	DSC	220.0(Huang et al., 2011)
71	JOTNOX	1644578-17-5	--	--	--	249.9(5)(Yin et al., 2014)	DSC	203.6(Yin et al., 2014)
72	ONAVEF01	26670-16-6	--	--	--	266.0(5)(Yang et al., 2016)	DSC	250.0(Yang et al., 2016)
73	MUKREQ	1198599-36-8	--	--	--	223.5(10)(Zeng et al., 2009)	DSC	--
74	LUFXUH	1819967-31-1	--	--	--	405.0(10)(Liu et al., 2015)	DSC	--
75	IBOPEW	33491-88-2	--	7.33(●)(Keshavarz, 2007)	--	362.0(decomp)(Zeman et al., 2010)	--	362.0(decomp)(Zeman et al., 2010)

76	ZUQWIT	133502-79-1	--	--	--	299.0(5)(Wei et al., 2015)	DSC	--
77	OSEWEQ	38082-89-2	--	--	--	360.0(5)(Klapötke et al., 2016)	DSC	360(Fried, 1998)
78	OTIBAW	55148-03-3	--	--	--	369.5(10)(Zhang et al., 2017)	DSC	--
79	LEGYII	2134229-83-5	--	--	--	261.2(5)(Yin et al., 2017)	DSC	--
80	GEYRAG	293324-58-0	--	--	--	307.0(5)(Tang et al., 2018)	DSC	304.0(Tang et al., 2018)
81	GEYQUZ	NA	--	--	--	280.0(5)(Tang et al., 2018)	DSC	278.0(Tang et al., 2018)
82	LEGYAA	2134229-85-7	--	--	--	307.2(5)(Yin et al., 2017)	DSC	--
83	GEYREK	NA	--	--	--	328.0(5)(Tang et al., 2018)	DSC	325.0(Tang et al., 2018)
84	KUBVEL	NA	--	--	--	351.0(5)(Li et al., 2019)	DSC	--
85	KUBVOV	NA	--	--	--	261.9(5)(Li et al., 2019)	DSC	--
86	HEVRUV	517-25-9	--	--	--	128(Saraf et al., 2003)	DSC	15.4(Goebel et al., 2006)
87	AWAKIT	14435-92-8	--	--	--	400(Li et al., 2015)	--	--

88	AZCYHO	24824-15-5	--	--	--	--		--
89	BIZKOM01	1564257-34-6	--	--	--	124(Kettner et al., 2014)	DSC	--
90	CAZCEN	125363-08-8	--	--	--	--	--	--
91	CIHQIT	155438-10-1				--	--	56(Qu et al., 2018)
92	CUGDIR	99393-63-2	--	--	--	200(Zhang et al., 2002)	DSC	>200(Wikipedia, 2006)
93	DIXDET	268748-97-6	--	--	--	--	--	--
94	DIXFEV	137538-62-6	--	--	--	--	--	--
95	EJEGIJ	155438-13-4	--	--	--	300(Sinditskii et al., 2016)	--	--
96	EJEGOP	260963-78-8	--	--	--	--	--	--
97	EJEGUV	155438-14-5	--	--	--	--	--	70(Sheremetev et al., 1998)
98	EJEHAC	612518-65-7	--	--	--	--	--	147(Averkiev et al., 2003)
99	FEPVON	1415050-06-4	--	--	--	176(Chavez et al., 2012)	DSC	124(Chavez et al., 2012)
100	FORMOQ	1638095-71-2	--	--	--	140(Fischer et al., 2014)	DSC	--
101	GEPRAU	210626-81-6	--	--	--	--	--	--

102	LITSIQ	292856-78-1	--	--	--	--	--	--
103	NIYDUU	206446-59-5	--	--	--	149.9(10)(Liu et al., 2015)	DSC	97.4(Liu et al., 2015)
104	OXAYES	162111-36-6	--	--	--	212(Veauthier et al., 2010)	DSC	127(Veauthier et al., 2010)
105	QQQBRD02	918-37-6	689(●)(Meyer et al., 2007)	7.58(●)(Pepekin et al., 2011)	23.6(●)(Pepekin et al., 2011)	136.1(Huang et al., 2015)	DSC	150(Wikipedia, 2006)
106	RABSUE	157628-84-7	--	--	--	220(decomp)(Makhova et al., 2003)	--	220(decomp)(Makhova et al., 2003)
107	RABTAL	155438-27-0	--	--	--	--	--	--
108	RAVSOW	33406-97-2	--	--	--	--	--	--
109	REQYIW	174092-36-5	--	--	--	--	--	235(Sheremetev et al., 1996)
110	SEJHEU	162111-38-8	--	--	--	232.23(Li et al., 2009)	DSC	230(Li et al., 2009)
111	TIBKAQ	155438-28-1	--	--	--	--	--	--
112	TIBKEU	178043-06-6	--	--	--	--	--	--
113	TIZMAQ	152845-81-3	--	--	--	190(Sinditskii et al., 2016)	--	63(Sheremetev et al., 1998)
114	UBAWUR	371227-83-7	--	--	--	148(Leonard et al., 2011)	DSC	99(Leonard et al., 2011)

115	UHAMAR	152845-82-4	--	--	--	--	--	112(Sheremetev et al., 1998)
116	UHOYIB	155256-96-5	--	--	--	--	--	103(Sheremetev et al., 2015)
117	ZULDOZ	17557-81-2	--	--	--	--	--	40(Ulpiani, 1912)
118	HNOBEN	15834-75-0	1650(●)(Rice and Hare, 2002)	9.30(●)(Keshavarz, 2008)	42.1(●)(Dong and Zhou, 1989)	261.9(Zeman, 1980)	DTA	240(Nielsen et al., 1979)
119	FEYMEC	29306-57-8	--	--	--	--	--	131(Manelis et al., 2006)
120	BZOFOX	3470-17-5	1410(●)(Dong and Zhou, 1989)	8.26(●)(Keshavarz, 2008)	35.1(○)(Akst, 1989)	289(10)(Yang et al., 2012)	DSC	193(Ohta et al., 1963)
121	AFUGEP	782438-60-2	--	8.68(●)(Tian et al., 2011)	36.1(●)(Tian et al., 2011)	186.0(10)(Zhang et al., 2014)	DSC	82.6(Zhang et al., 2014)
122	XERPAM	371951-09-6	1383.6(●)(Zhou et al., 2011)	8.93(●)(Zhou et al., 2011)	--	272.0(5)(LI et al., 2016)	DSC	109.0(LI et al., 2016)
123	BADNAY01	1809272-88-5	--	--	--	138.0(Terrier et al., 1990)	--	--

124	SEFVOR	2195346-95-1	--	--	--	233.1(5)(Tang et al., 2017)	DSC	205.5(Tang et al., 2017)
125	PUBMII01	189192-28-7	--	--	--	> 195(decomp)(Meyer et al., 2016)	--	> 195(decomp)(Meyer et al., 2016)
126	DEDBUJ	98686-54-5	--	--	--	--	--	--
127	HIQBER	152678-74-5	--	--	--	243.0(5)(Kumar et al., 2018)	DSC	209.0(Kumar et al., 2018)
128	VETWAS	131394-26-8	--	--	--	290.0(5)(Liu et al., 2015)	DSC	--
129	DAZDUF	134293-22-4	--	--	--	214.0(5)(Fischer et al., 2012)	DSC	--
130	FIHPIY	2243211-28-9	--	--	--	228.0(5)(Tang et al., 2018)	DSC	--
131	KUBVIP	NA	--	--	--	340.8(5)(Li et al., 2019)	DSC	--
132	FOXHIM	131846-99-6	--	--	--	329(5)(Zhang et al., 2019)	DSC	--
133	OYAVIV	2095393-79-4	--	--	--	335.0(5)(Klapötke and Witkowski, 2016)	DSC	--
134	ZASWEX	2387677-24-7	--	--	--	--	--	--
135	ZASWAT	2387677-23-6	--	--	--	--	--	--

136	CUJFAQ	1801269-93-1	--	--	--	302.0(5)(Klapötke and Witkowski, 2016)	DSC	--
137	GEYQOT	NA	--	--	--	261.0(5)(Tang et al., 2018)	DSC	233.0(Tang et al., 2018)
138	MUKRAM	1198599-46-0	--	--	--	298.3(10)(Zeng et al., 2009)	DSC	
139	FOYSUJ	NA	--	--	--	197.9(Wu et al., 2015)	DSC	156.6(Wu et al., 2015)
140	CUDQUP	29754-26-5	--	--	--	260(10)(Hong et al., 2015)	DSC	67(10)(Hong et al., 2015)
141	GEXMON	1418127-35-1	--	--	--	--	--	171.3(10)(Zhang et al., 2013)
142	GEXMIH	1418127-36-2	--	--	--	--	--	205.8(10)(Zhang et al., 2013)
143	GEXMAZ	1418127-37-3	--	--	--	--	--	132.6(10)(Zhang et al., 2013)
144	GEXMED	1418127-38-4	--	--	--	--	--	189.0(10)(Zhang et al., 2013)
145	ZEVNUL	NA	--	--	--	--	--	164.5(10)(Zhang et al., 2013)
146	PEHSUS	2309306-47-4	--	--	--	235(10)(Yang et al., 2012)	DSC	220(Yang et al., 2012)
147	TOZMUS	NA	--	--	--	240(10)(Hong et al., 2015)	DSC	62(10)(Hong et al., 2015)

148	IZUZUZ	1583315-32-5	--	--	--	207(10)(Bolton et al., 2011)	DSC	136(10)(Bolton and Matzger, 2011)
149	TIVJUF	2387677-27-0	--	--	--	216.8(10)(Wang et al., 2014)	DSC	136.7(10)(Wang et al., 2014)
150	QISTAN01	250165-39-0	--	--	--	--	--	--
151	GOWHIL	NA	--	--	--	220(10)(Yang et al., 2014)	DSC	91(10)(Yang et al., 2014)
152	ZEBJOH	1668570-32-8	--	--	--	243.5(10)(Gao et al., 2014)	DSC	-
153	FIHPEU	2243696-54-8	--	--	--	315.1(5)(Tang et al., 2018)	DSC	--

Table S4. Feature importance ranking by the magnitude of Pearson correlation coefficients. (Related to Figure 5)

Label	Feature	*Importance to Q_{max}*	Feature	*Importance to D*	Feature	*Importance to $p_{C\text{-}J}$*	Feature	*Importance to T_d*	Feature	*Importance to LE*
1	Product gaseous CO_2	0.610	Product solid C	-0.813	Product solid C	-0.820	Oxygen balance	-0.430	Incrystal mix with hydrogen-rich molecules	0.698
2	HB strength	-0.597	Oxygen balance	0.806	Oxygen balance	0.803	HB amount	0.390	HB strength	0.603
3	Functional group - NH_2	-0.472	Material density	0.748	Material density	0.794	Weakest bond strength	0.378	HB amount	0.564
4	Product gaseous H_2O	-0.378	Product gaseous CO_2	0.691	Product gaseous CO_2	0.700	HB length	0.287	Incrystal mix with energetic molecules	0.536
5	Product gaseous O_2	-0.367	Product gaseous N_2	0.544	Product gaseous N_2	0.549	Molecular weight	0.227	HB length	0.308
6	HB amount	-0.324	Crystal packing coefficient	0.362	Crystal packing coefficient	0.407	Number of molecules in a	-0.219	Material density	-0.288

							primitive cell			
7	Crystal packing type	0.307	Nitrogen density	0.290	Nitrogen density	0.301	Material density	-0.217	Molecular weight	0.274
8	Product gaseous NH_3	-0.300	Product gaseous NH_3	-0.281	HB amount	-0.265	Crystal packing type	-0.194	Oxygen balance	-0.272
9	HB length	-0.267	HB amount	-0.260	Functional group -NO_2	0.260	Functional group -NH_2	0.191	Weakest bond strength	0.245
10	Molecular weight	0.251	Incrystal mix with energetic molecules	-0.259	Incrystal mix with energetic molecules	-0.254	HB strength	0.190	Weakest bond type	-0.198
11	Oxygen balance	0.201	HB strength	-0.243	Product gaseous NH_3	-0.254	Weakest bond length	0.189	Molecular backbone	0.183
12	Product gaseous N_2	0.193	Functional group -NO_2	0.238	HB strength	-0.226	Functional group -N_3	0.185	Functional group -NH_2	0.148

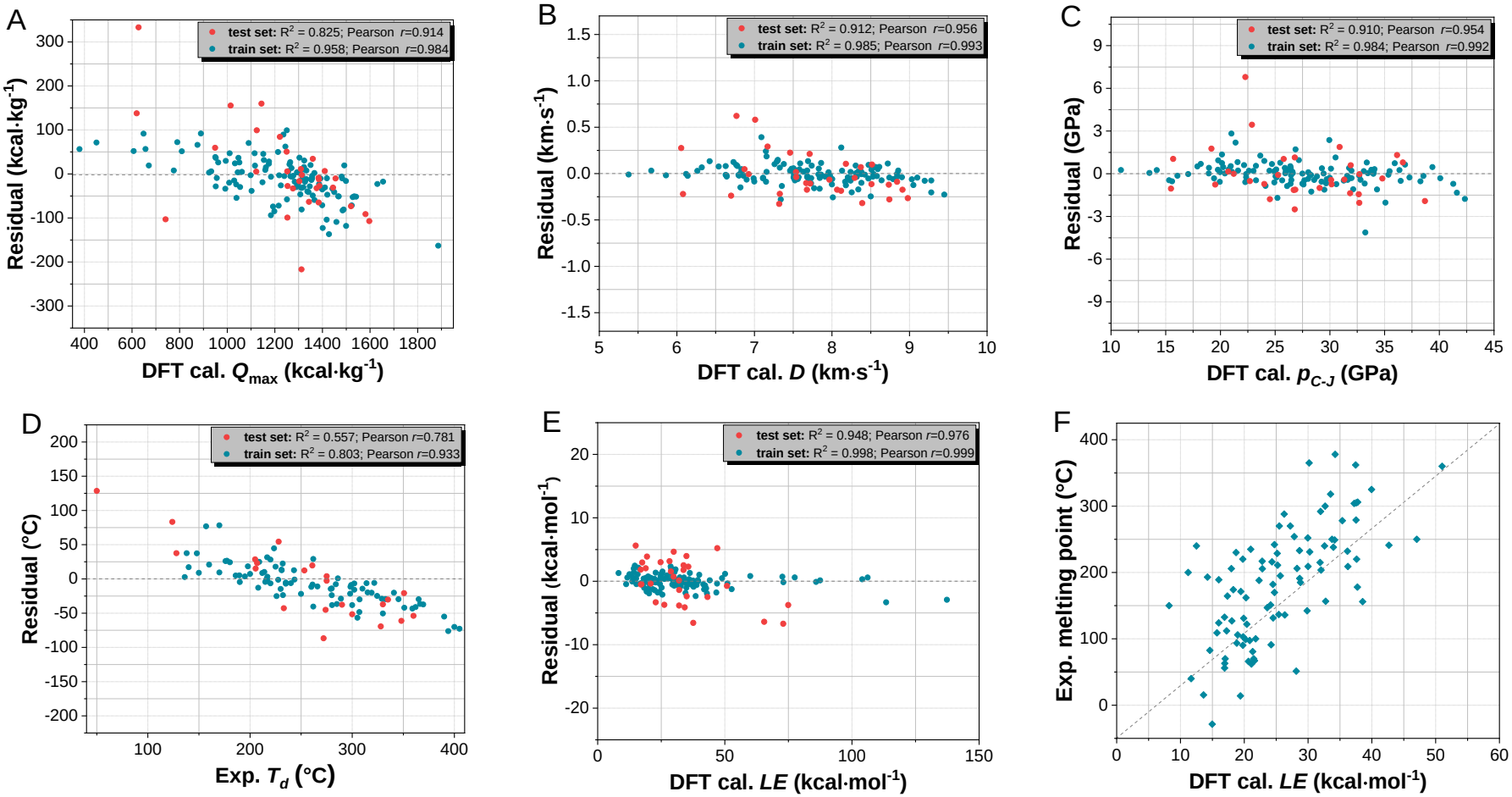

Figure S1. XGBoost prediction residuals for (A) Q_{max}, (B) D, (C) $p_{C\text{-}J}$, (D) T_d, and (E) LE. (F) Roughly positive correlation of melting temperature to LE. (Related to Table 1 and Figure 4)

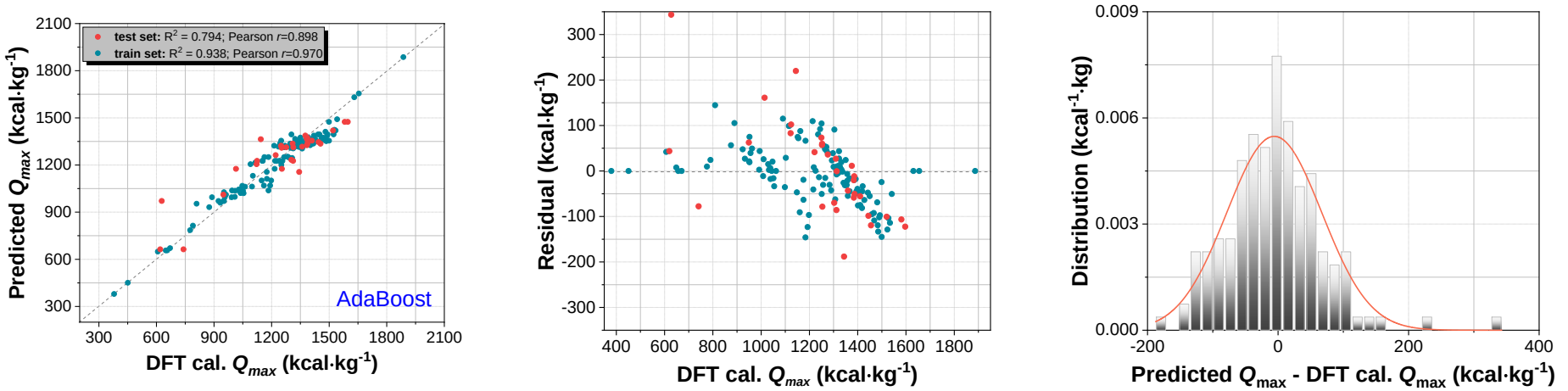

Figure S2. Prediction of heat of explosion with AdaBoost model. (Related to Table 1)

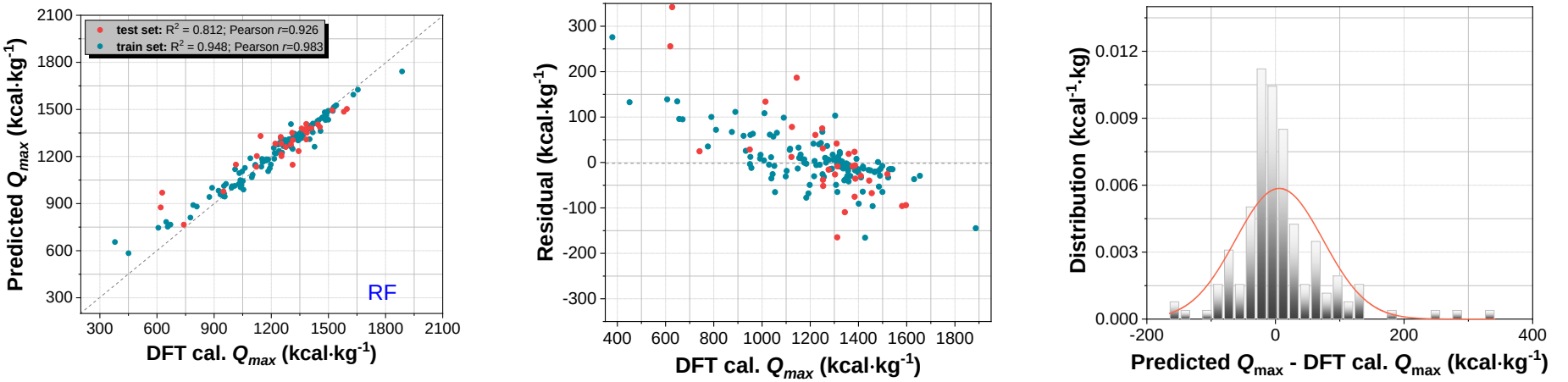

Figure S3. Prediction of heat of explosion with RF model. (Related to Table 1)

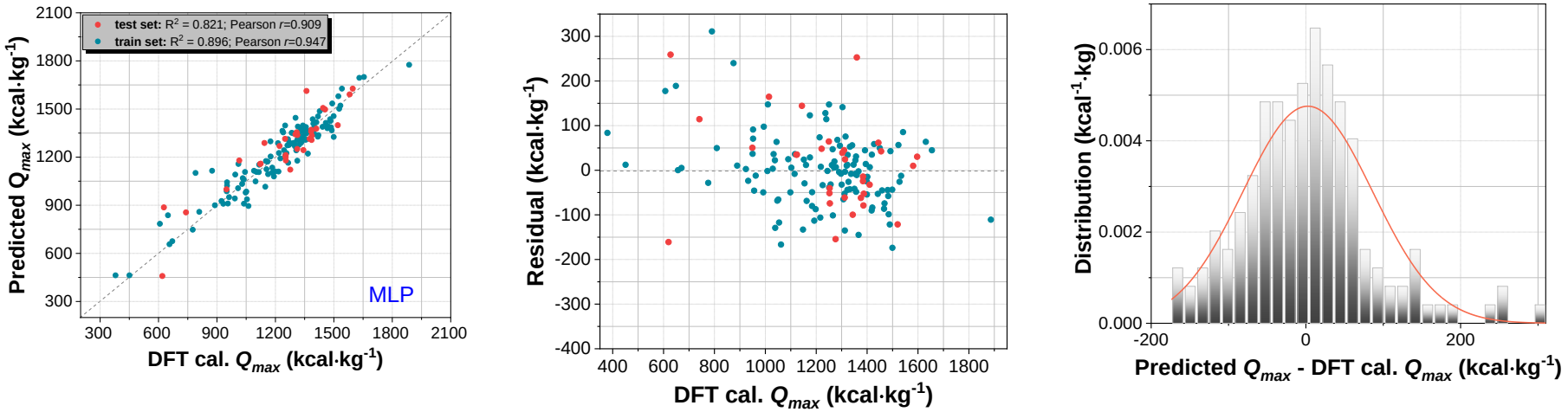

Figure S4. Prediction of heat of explosion with MLP model. (Related to Table 1)

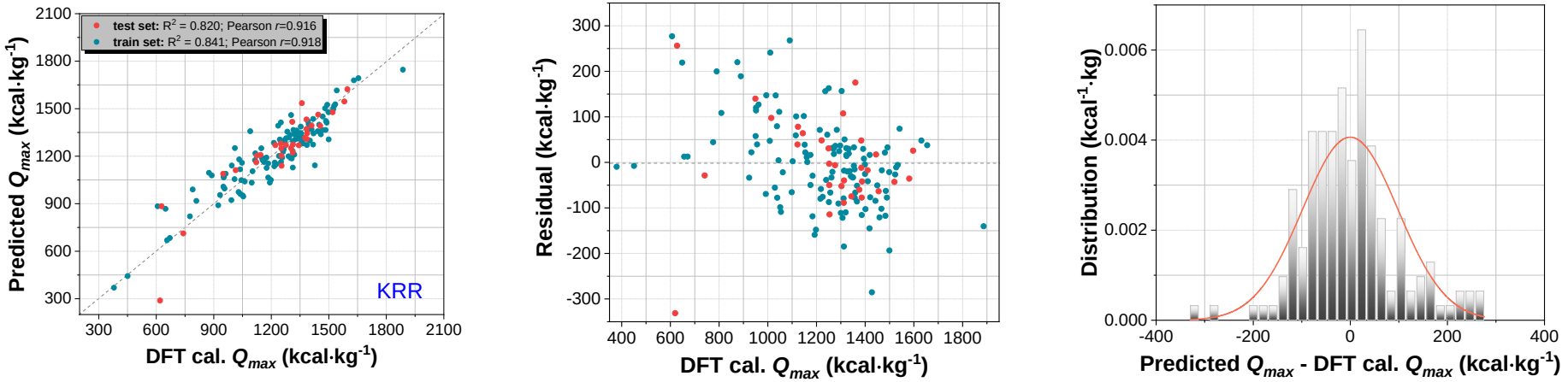

Figure S5. Prediction of heat of explosion with KRR model. (Related to Table 1)

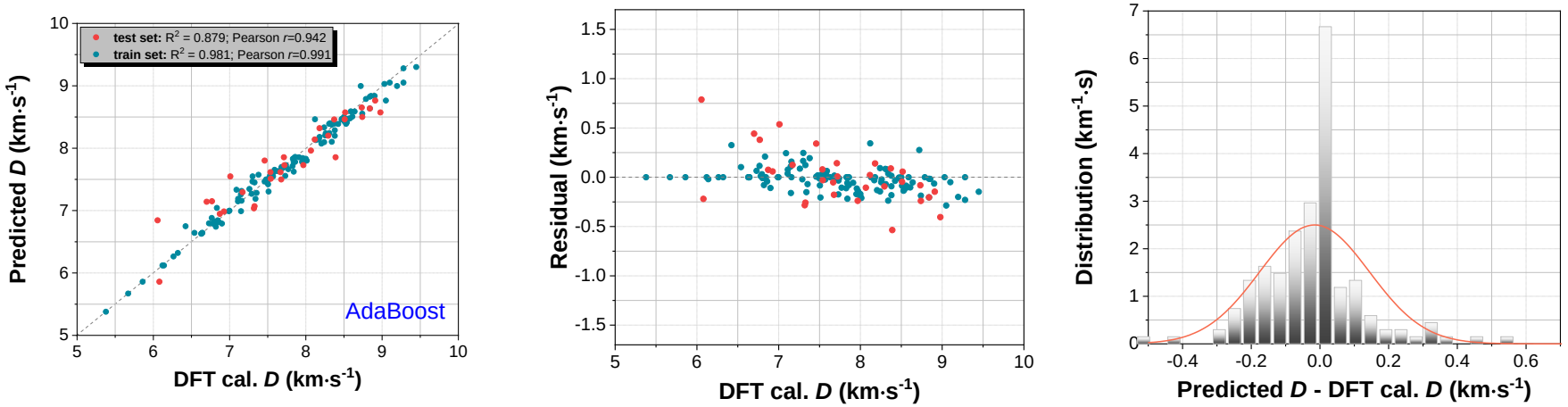

Figure S6. Prediction of detonation velocity with AdaBoost model. (Related to Table 1)

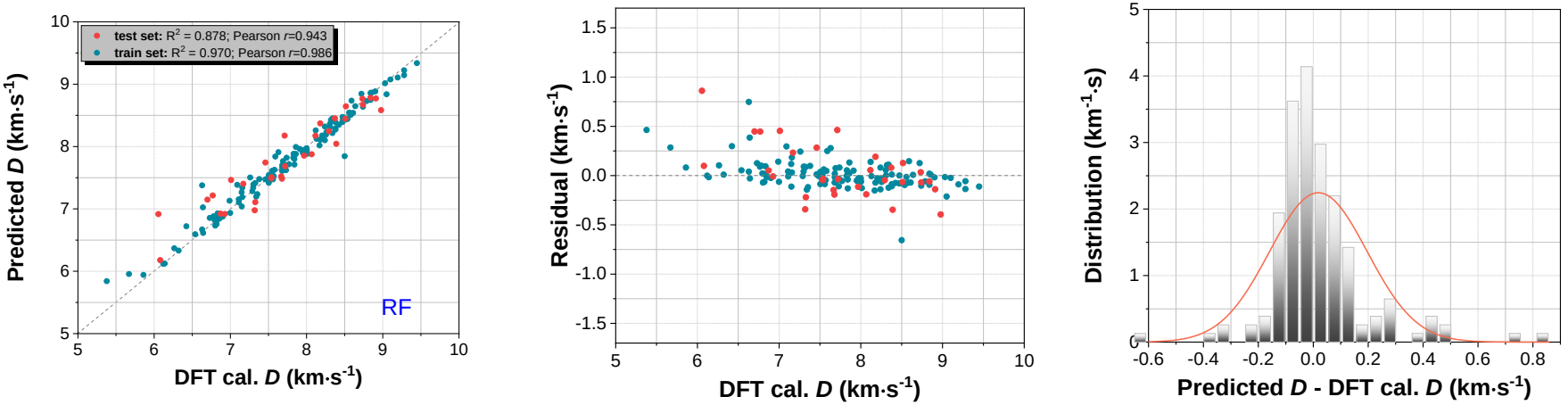

Figure S7. Prediction of detonation velocity with RF model. (Related to Table 1)

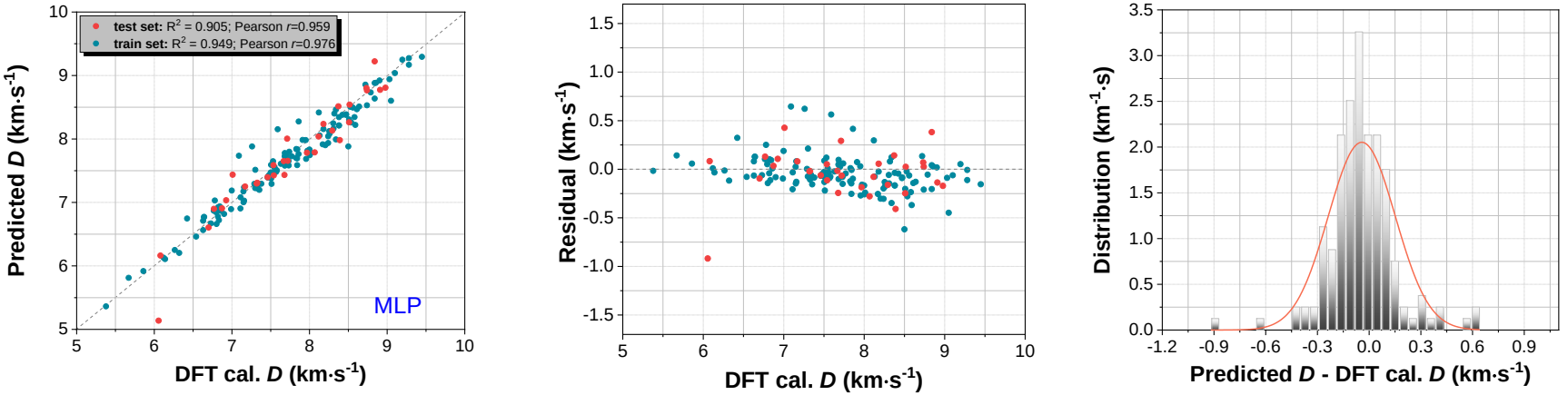

Figure S8. Prediction of detonation velocity with MLP model. (Related to Table 1)

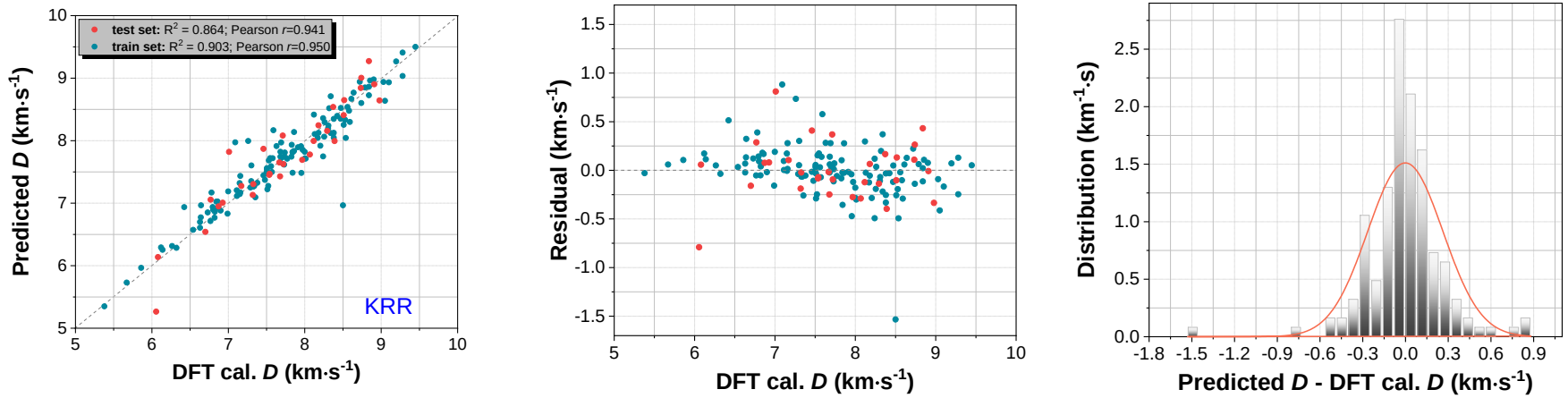

Figure S9. Prediction of detonation velocity with KRR model. (Related to Table 1)

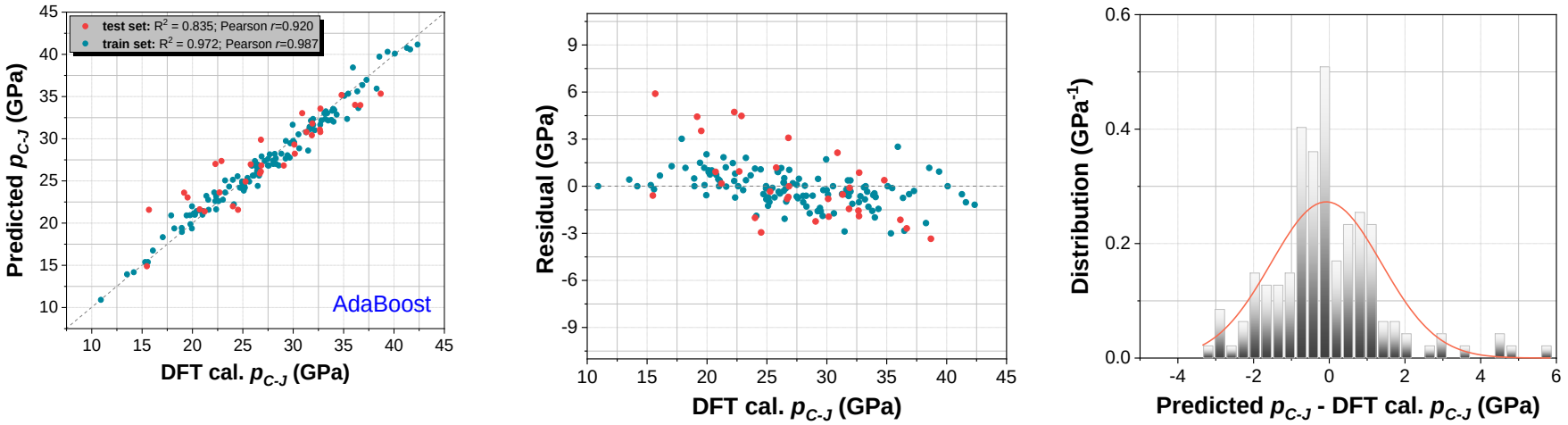

Figure S10. Prediction of detonation pressure with AdaBoost model. (Related to Table 1)

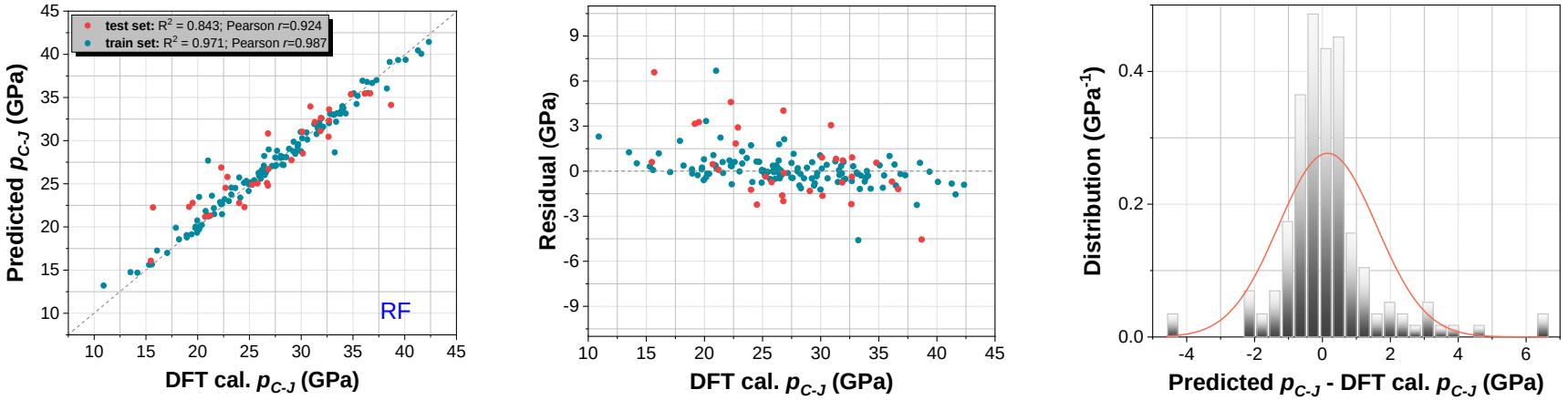

Figure S11. Prediction of detonation pressure with RF model. (Related to Table 1)

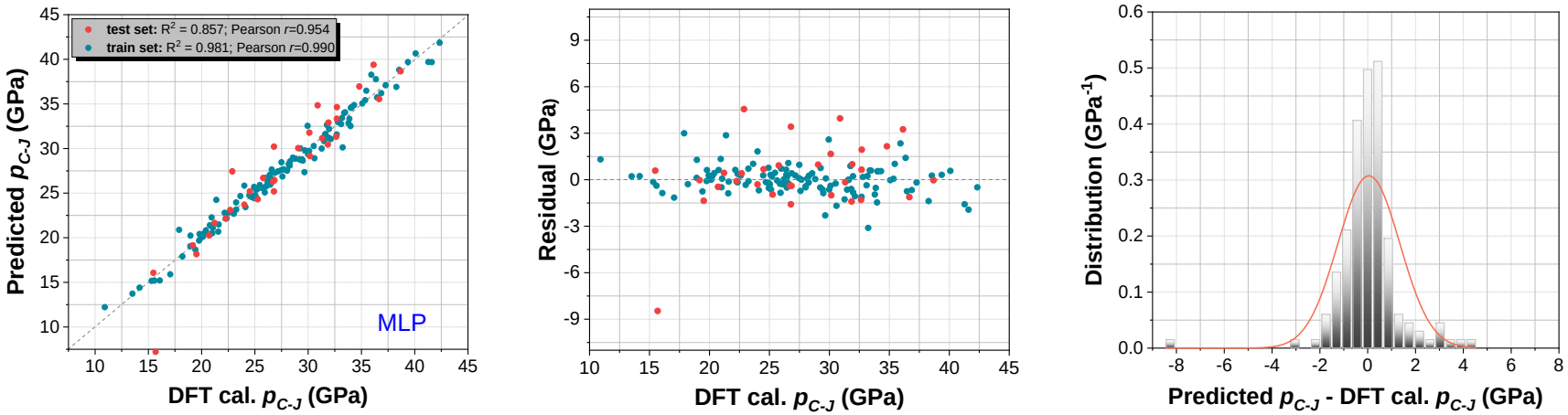

Figure S12. Prediction of detonation pressure with MLP model. (Related to Table 1)

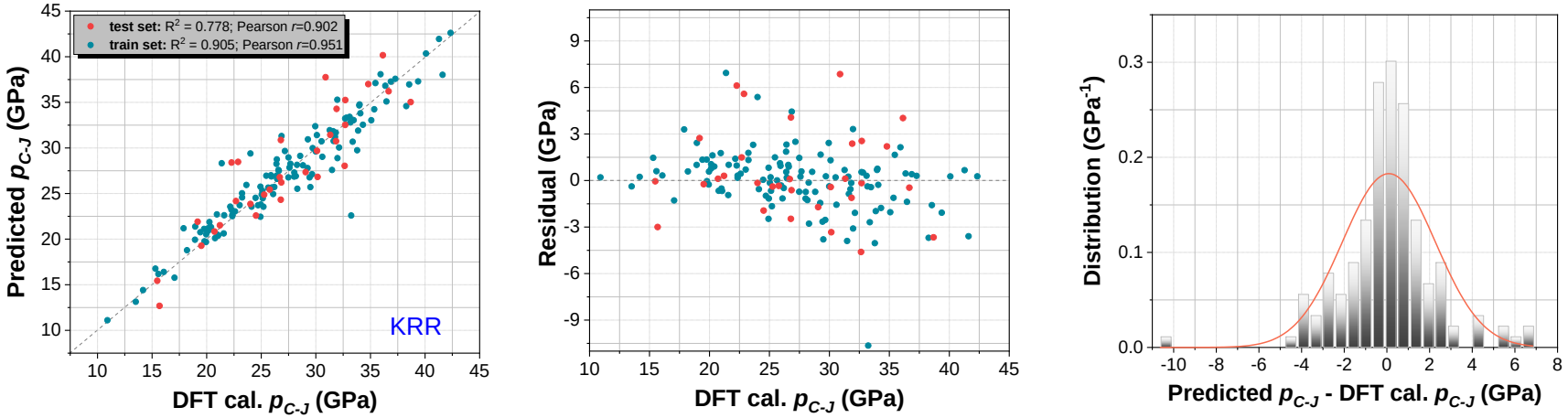

Figure S13. Prediction of detonation pressure with KRR model. (Related to Table 1)

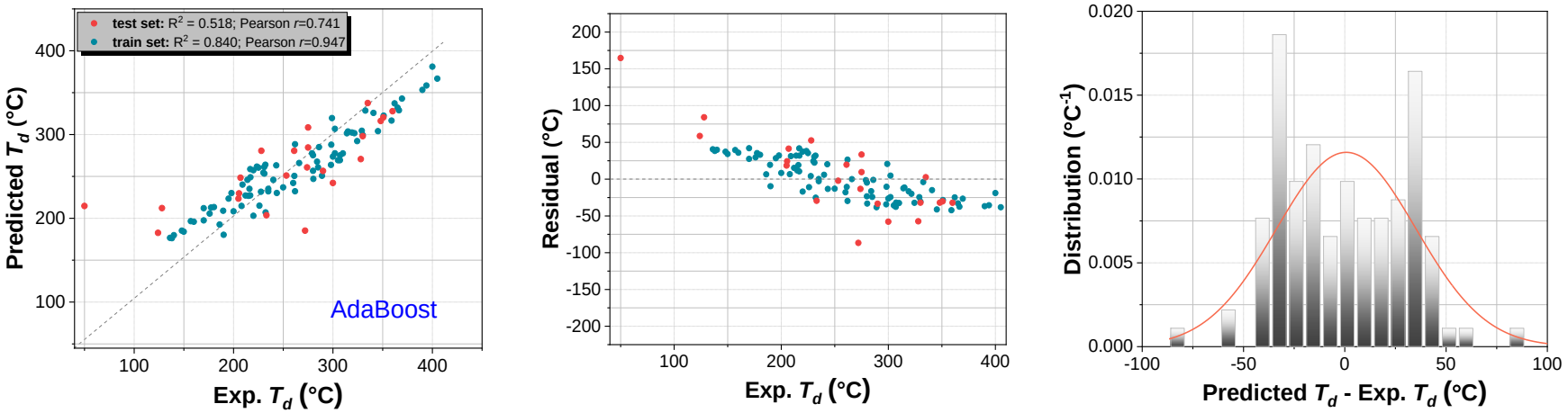

Figure S14. Prediction of decomposition temperature with AdaBoost model. (Related to Table 1)

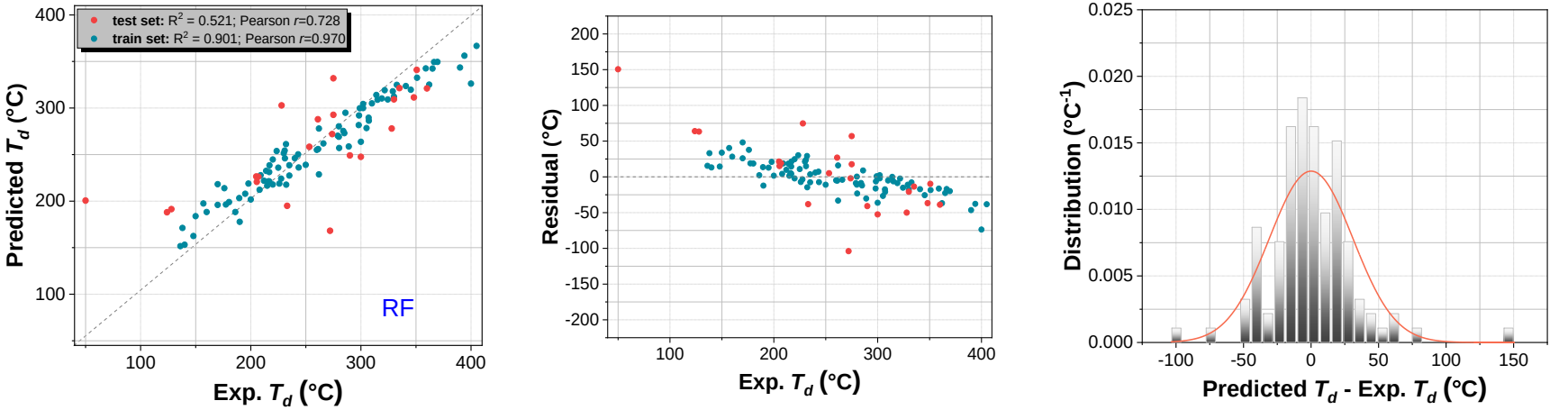

Figure S15. Prediction of decomposition temperature with RF model. (Related to Table 1)

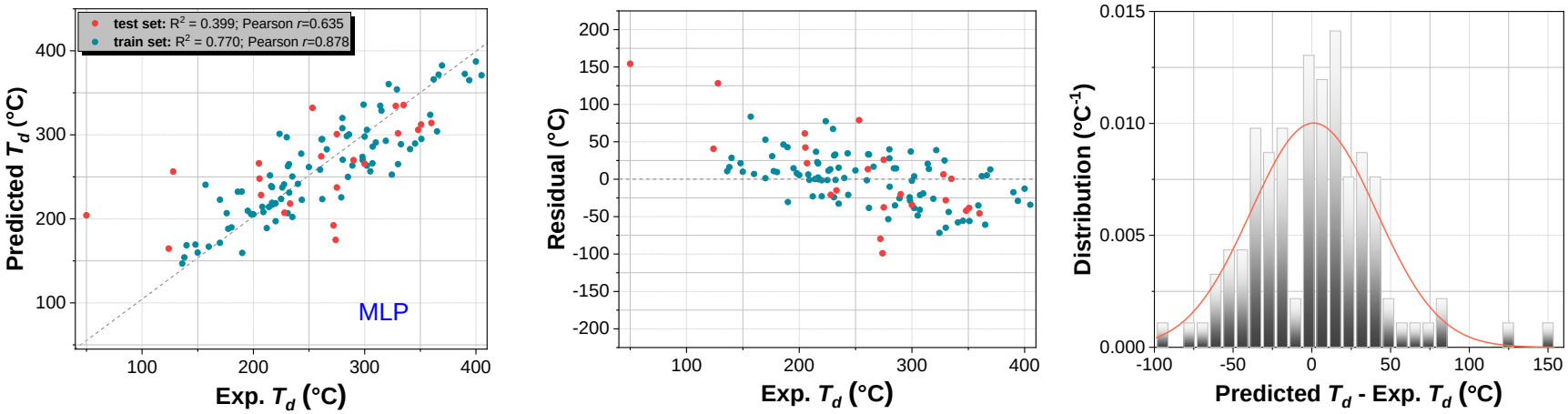

Figure S16. Prediction of decomposition temperature with MLP model. (Related to Table 1)

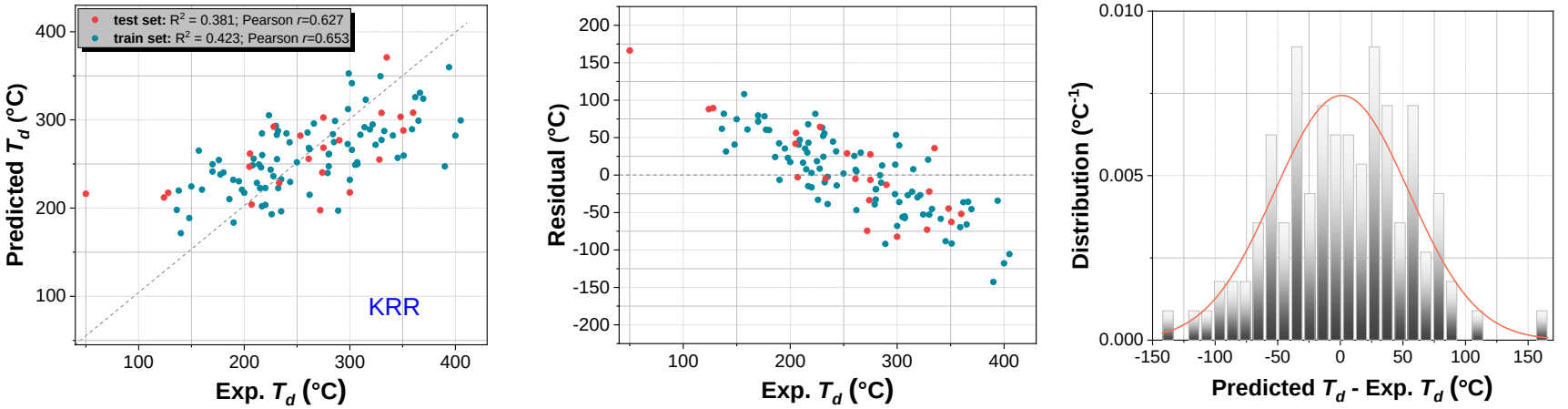

Figure S17. Prediction of decomposition temperature with KRR model. (Related to Table 1)

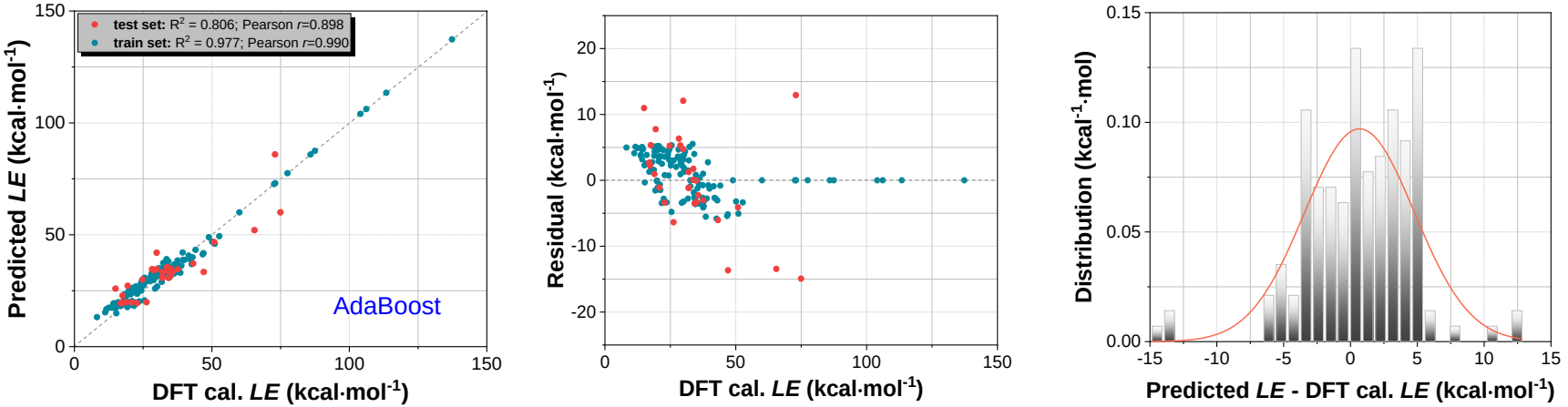

Figure S18. Prediction of lattice energy with AdaBoost model. (Related to Table 1)

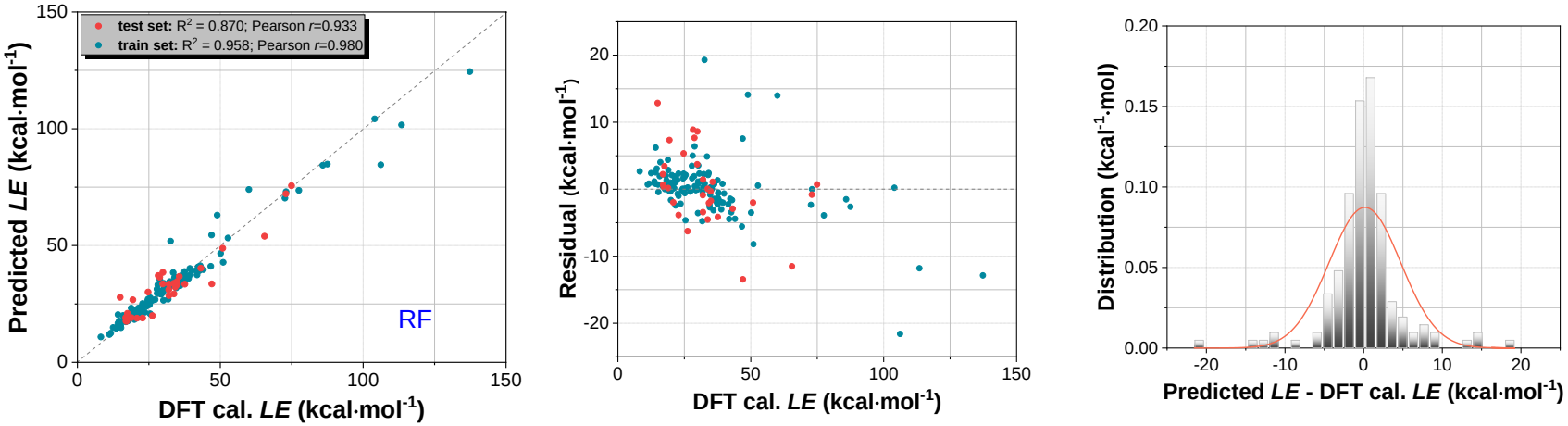

Figure S19. Prediction of lattice energy with RF model. (Related to Table 1)

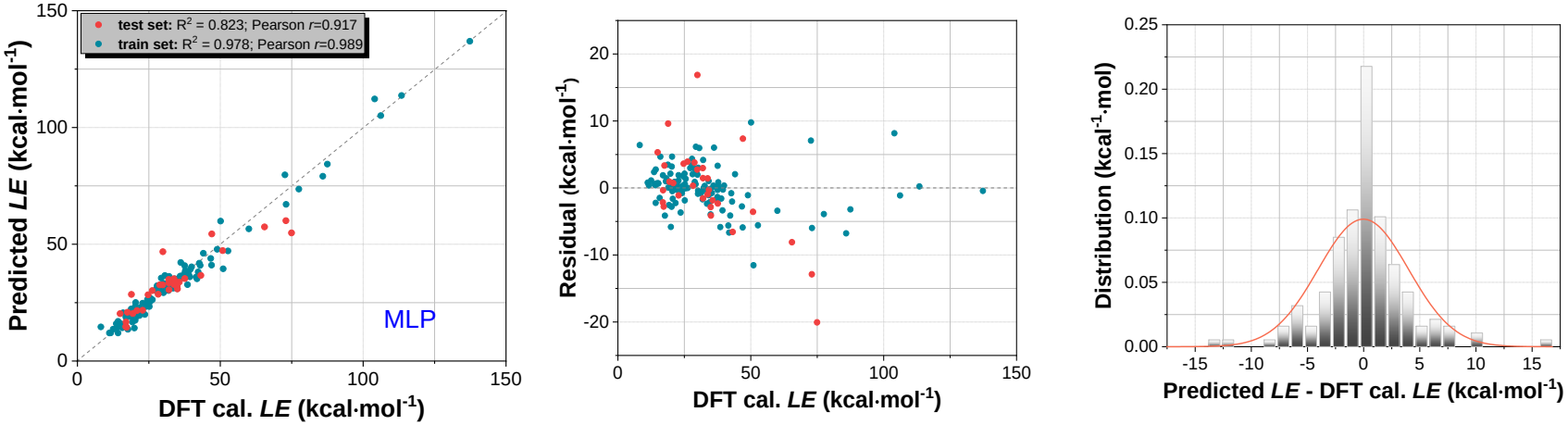

Figure S20. Prediction of lattice energy with MLP model. (Related to Table 1)

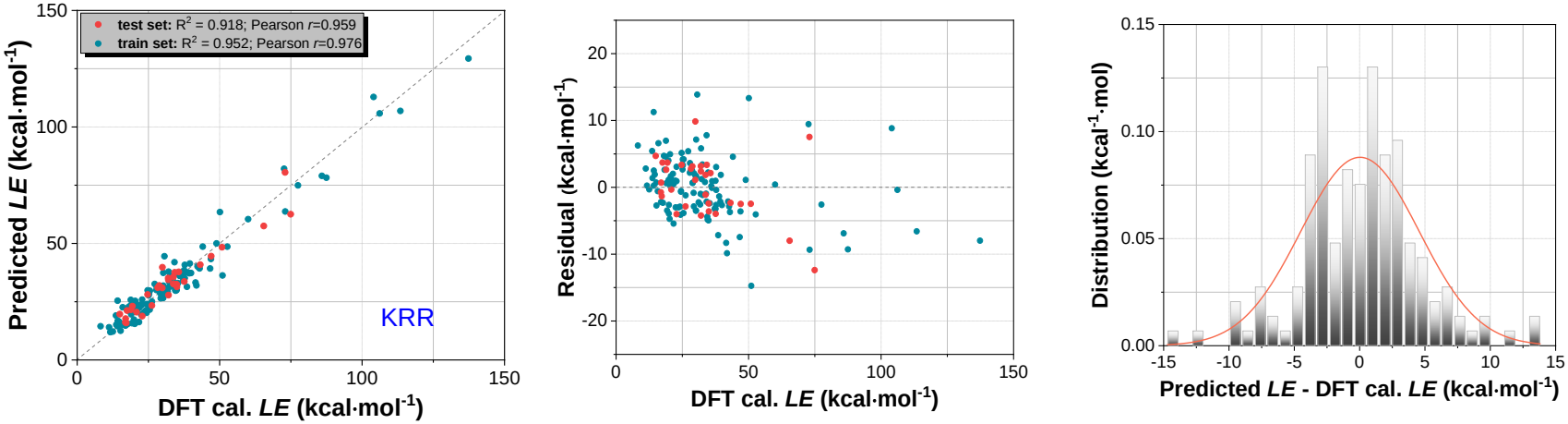

Figure S21. Prediction of lattice energy with KRR model. (Related to Table 1)

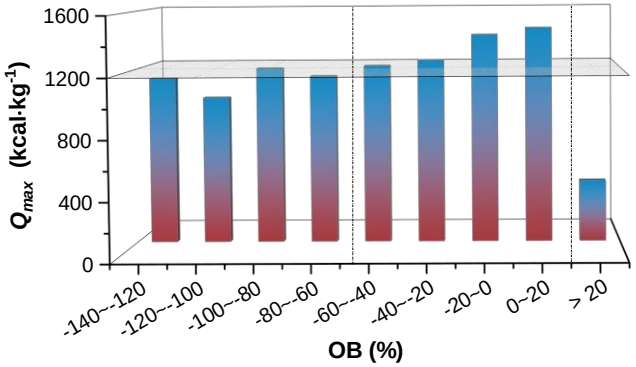

-60% < OB < 20%

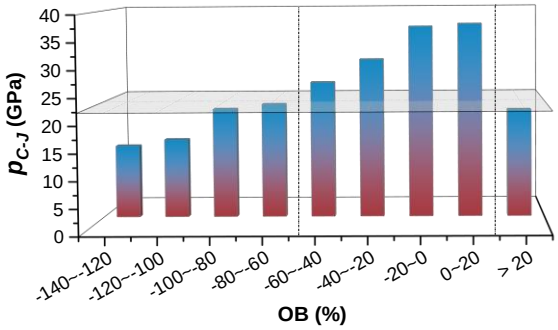

-60% < OB < 20%

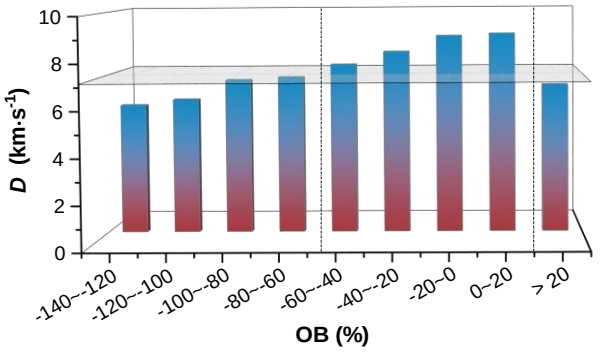

-60% < OB < 20%

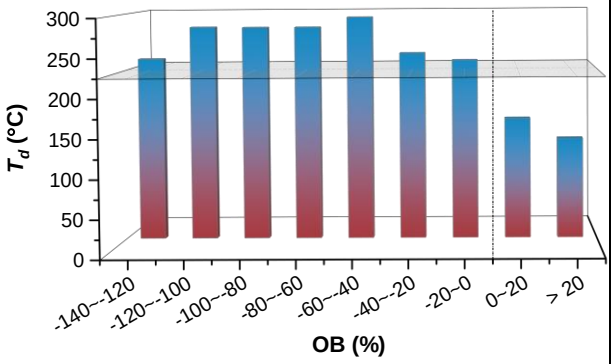

-140% < OB < 0%

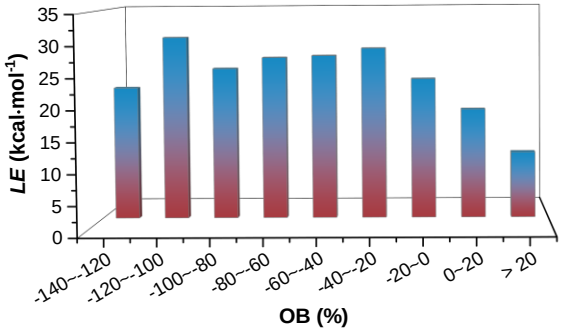

Weak relevance & Arbitrary range

Optimal range:

-60 < OB < 0%

Figure S22. Optimal range of oxygen balance in balancing detonation performance and stability of HEMDs. (Related to Table 2)

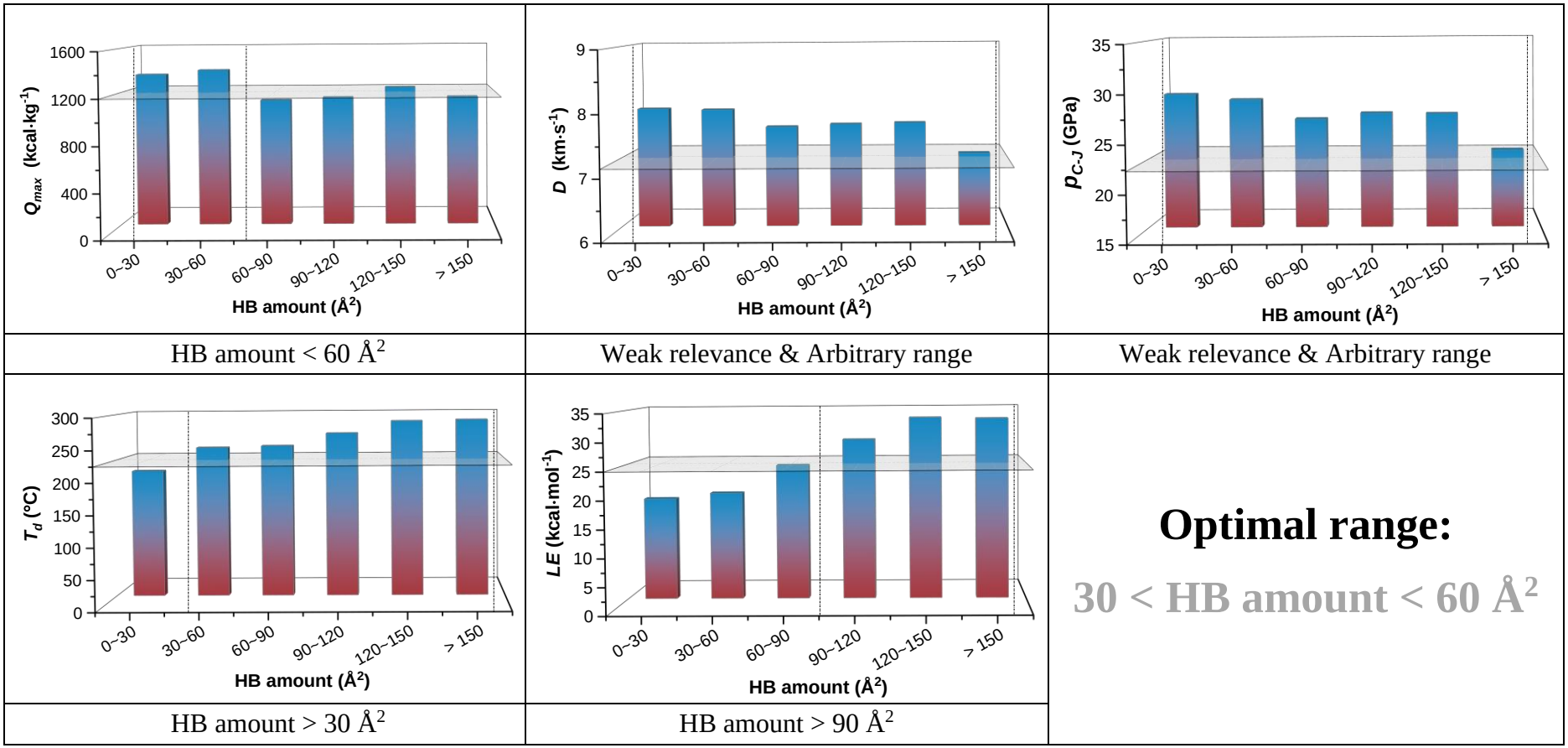

Figure S23. Optimal range of HB amount in balancing detonation performance and stability of HEMDs. (Related to Table 2)

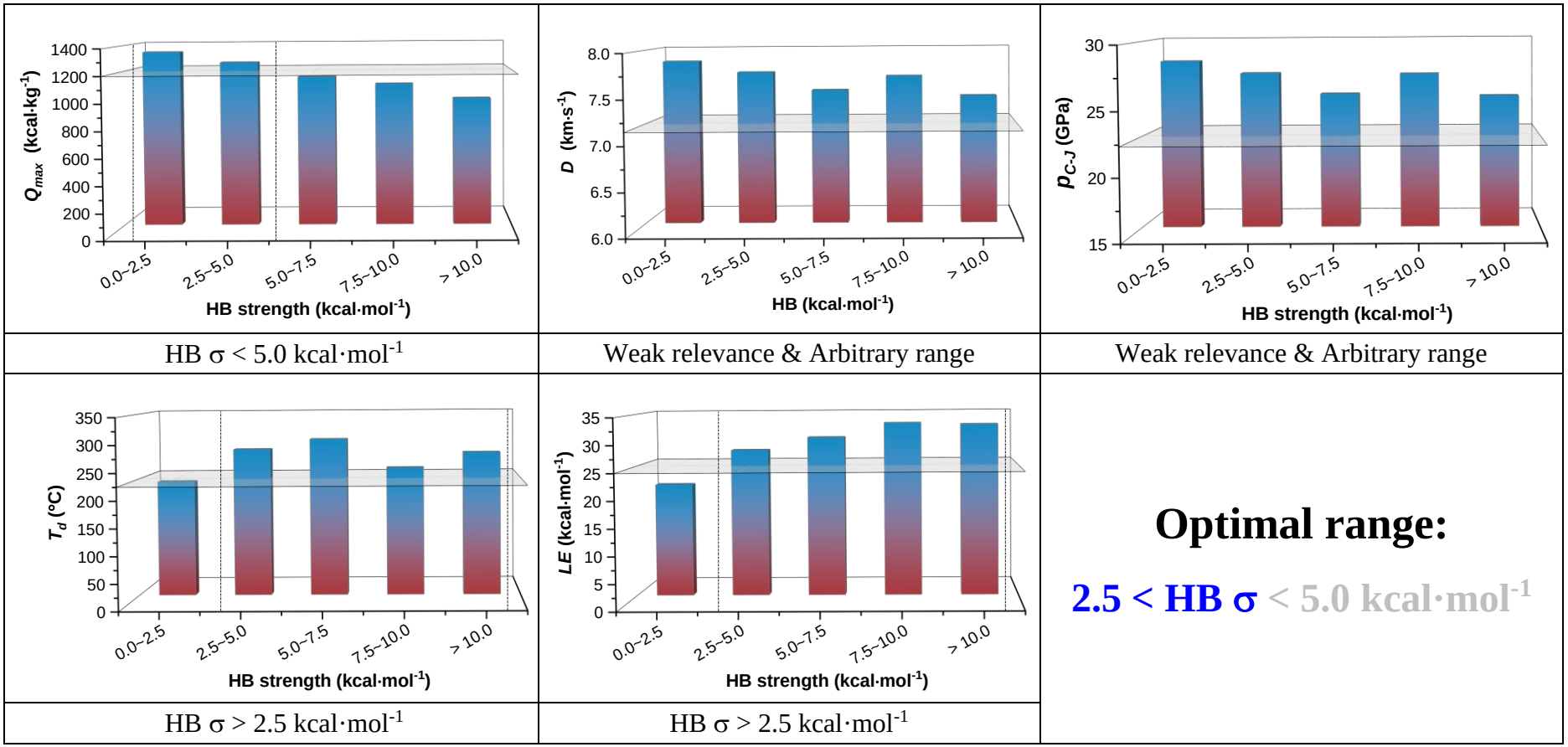

Figure S24. Optimal range of HB strength in balancing detonation performance and stability of HEMDs. (Related to Table 2)

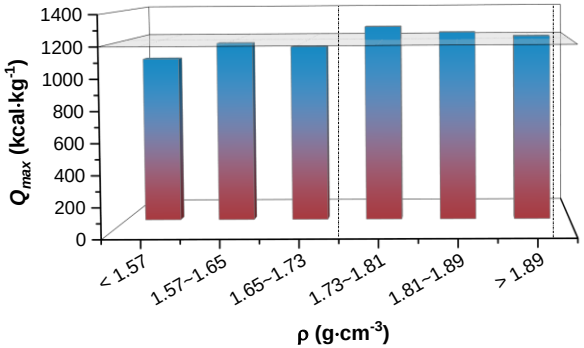

ρ > 1.73 g·cm^{-3}

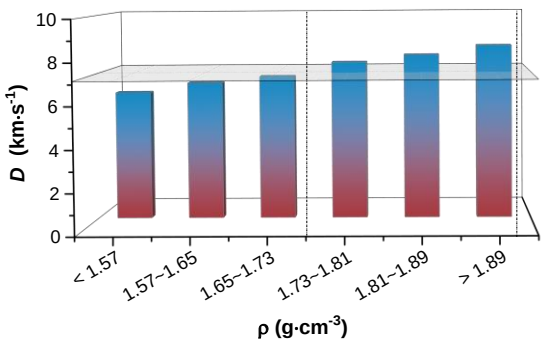

ρ > 1.73 g·cm^{-3}

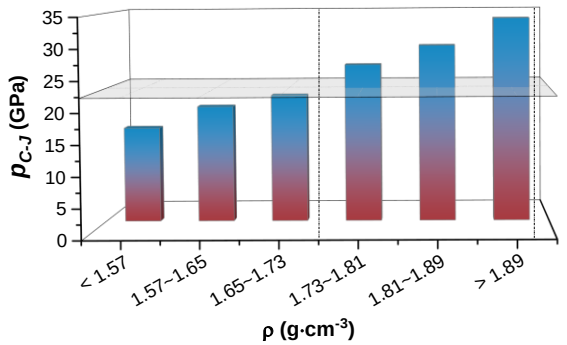

ρ > 1.73 g·cm^{-3}

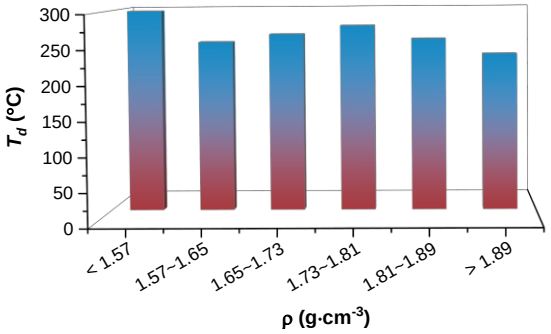

Weak relevance & Arbitrary range

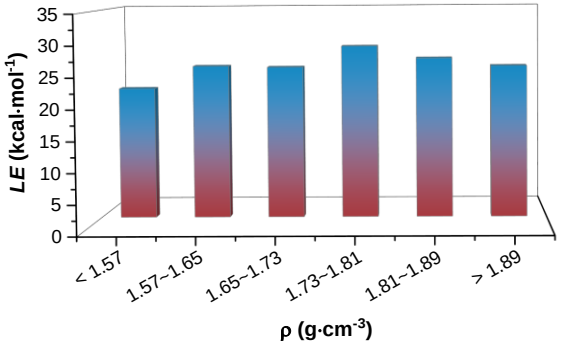

Weak relevance & Arbitrary range

Optimal range:

ρ > 1.73 g·cm^{-3}

Figure S25. Optimal range of material density in balancing detonation performance and stability of HEMDs. (Related to Table 2)

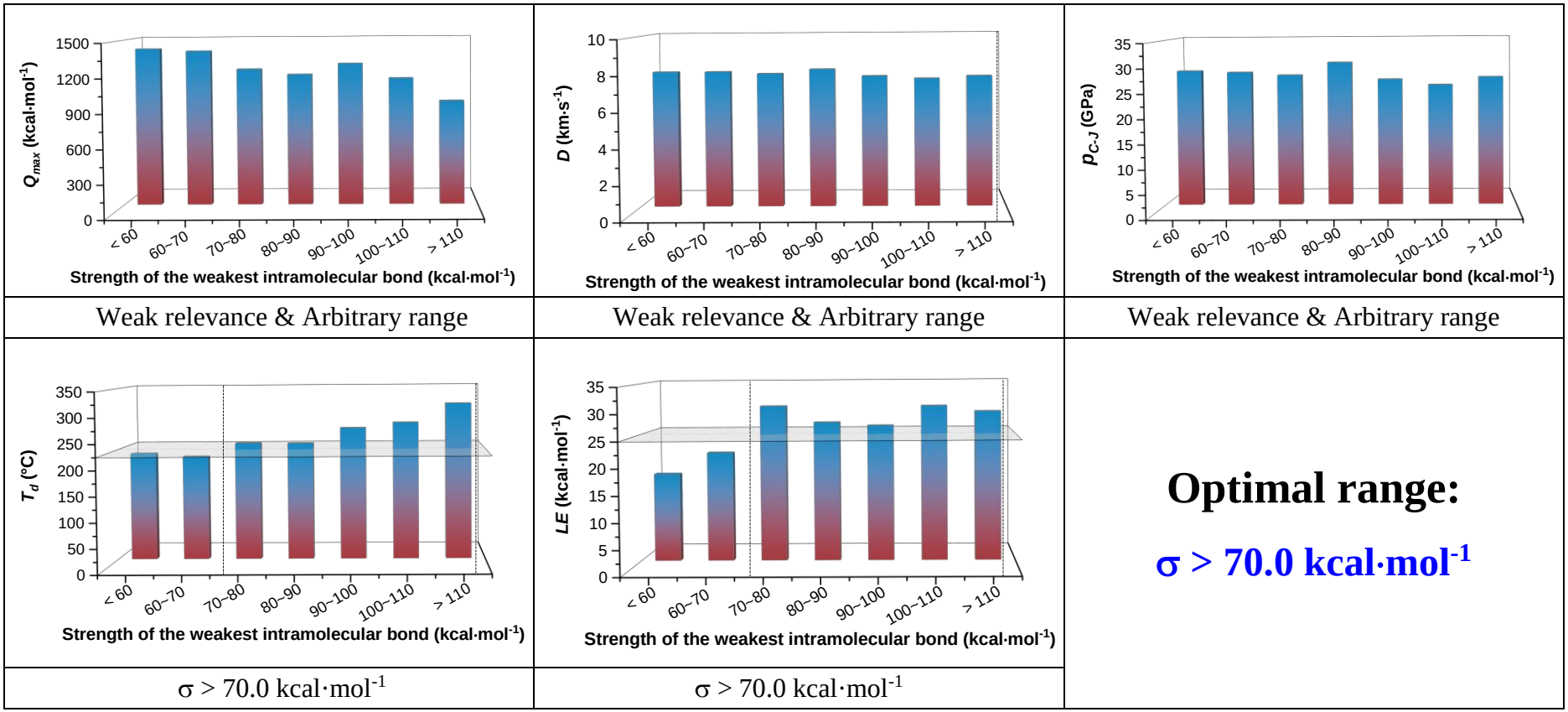

Figure S26. Optimal range of strength of the weakest intramolecular bond in balancing detonation performance and stability of HEMDs. (Related to Table 2)

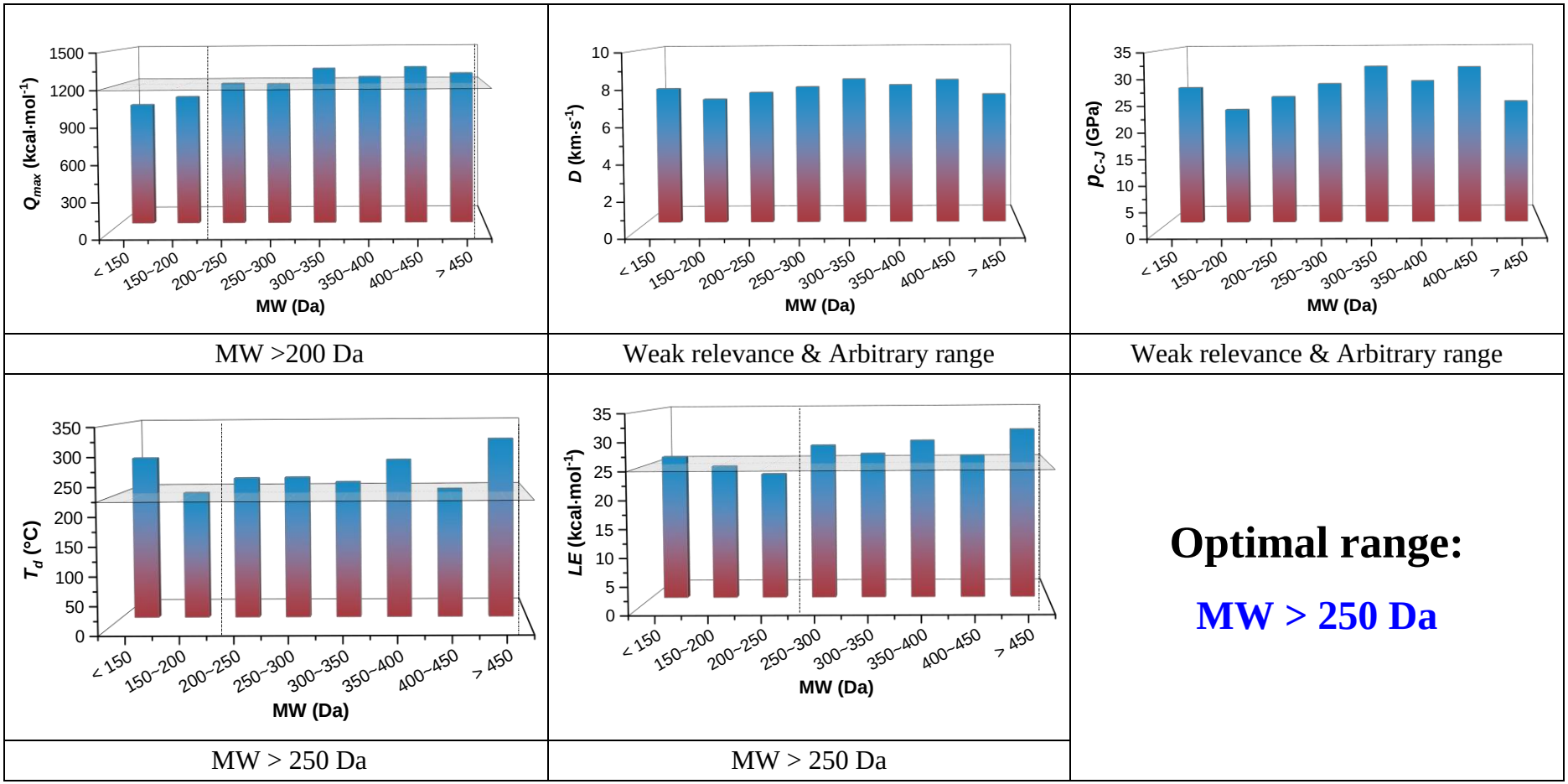

Figure S27. Optimal range of molecular weight in balancing detonation performance and stability of HEMDs. (Related to Table 2)

References

Akst, I. (1989). Heat of detonation, the cylinder test, and performance munitions. Los Alamos National Lab., NM (USA).

Altenburg, T., Klapötke, T.M., and Penger, A. (2009). Primary nitramines related to nitroglycerine: 1-nitramino-2, 3-dinitroxypropane and 1, 2, 3-trinitraminopropane. Cent. Eur. J. Energ. Mater. *6*, 255-275.

Altmann, K.L., Chafin, A.P., Merwin, L.H., Wilson, W.S., and Gilardi, R. (1998). Chemistry of tetraazapentalenes. J. Org. Chem. *63*, 3352-3356.

Antonangeli, D., Farber, D.L., Said, A.H., Benedetti, L.R., Aracne, C.M., Landa, A., Söderlind, P., and Klepeis, J.E. (2010). Shear softening in tantalum at megabar pressures. Phys. Rev. B *82*, 132101.

Atkins, R.L., Hollins, R.A., and Wilson, W.S. (1986). Synthesis of polynitro compounds. Hexasubstituted benzenes. J. Org. Chem. *51*, 3261-3266.

Averkiev, B., Antipin, M.Y., Yudin, I., and Sheremetev, A. (2002). X-ray structural study of three derivatives of dinitropyrazine. J. Mol. Struct. *606*, 139-146.

Averkiev, B.B., Antipin, M.Y., Sheremetev, A.B., and Timofeeva, T.V. (2003). Four 3-cyanodifurazanyl ethers: potential propellants. Acta Crystallogr. Sect. C: Cryst. Struct. Commun. *59*, o383-o387.

Bachman, G.B., and Vogt, C.M. (1958). The BF3· N2O4 complex as a nitrating agent1. J. Am. Chem. Soc. *80*, 2987-2991.

Bagryanskaya, I.Y., and Gatilov, Y.V. (1983). Crystal structure of nitromethane. J. Struct. Chem. *24*, 150-151.

Bemm, U., and Östmark, H. (1998). 1,1-diamino-2,2-dinitroethylene: A novel energetic material with infinite layers in two dimensions. Acta Crystal. *54*, 1997–1999.

Blanksma, J.J. (1908). Bromination and Nitration of Meta-Substituted Phenols. Rec. Trav. Chim. *27*, 25-41.

Boileau, J., Carail, M., Wimmer, E., Gallo, R., and Pierrot, M. (1985). Dérivés nitrés acétylés du glycolurile. Propellants, Explos., Pyrotech. *10*, 118-120.

Bölter, M.F., Klapötke, T.M., Kustermann, T., Lenz, T., and Stierstorfer, J. (2018). Improving the Energetic Properties of Dinitropyrazoles by Utilization of Current Concepts. Eur. J. Inorg. Chem. *2018*, 4125-4132.

Bolton, O., and Matzger, A.J. (2011). Improved stability and smart-material functionality realized in an energetic cocrystal. Angew. Chem. *123*, 9122-9125.

Boyer, J., and Morgan, J., L (1959). Acid catalyzed reactions between carbonyl compounds and organic azides. II. aromatic aldehydes. J. Org. Chem. *24*, 561-562.

Cai, H., Shu, Y., Huang, H., Cheng, B., and Li, J. (2004). Study on reactions of 2-(dinitromethylene)-4, 5-imidazolidinedione. J. Org. Chem. *69*, 4369-4374.

Chavez, D.E., Parrish, D.A., and Leonard, P. (2012). The synthesis and characterization of a new furazan heterocyclic system. Synlett *23*, 2126-2128.

Chaykovsky, M., and Adolph, H.G. (1990). Synthesis and properties of some trisubstituted trinitrobenzenes. TATB analogs. J. Energ. Mater. *8*, 392-414.

Colonna, G.R., and Spencer, A.B. (2010). Fire Protection Guide to Hazardous Materials (14th edition) (National Fire Protection Association).

Crawford, M.J., Evers, J., Göbel, M., Klapötke, T.M., Mayer, P., Oehlinger, G., and Welch, J.M. (2007).

γ - FOX - 7: Structure of a High Energy Density Material Immediately Prior to Decomposition. Propellants, Explos., Pyrotech. *32*, 478-495.

Davis, T.L., and Abrams, A.J. (1925). The Dehydration of Ammonium Nitrate. J. Am. Chem. Soc. *47*, 1043-1045.

Dobratz, B.M., and Crawford, P.C. (1985). LLNL explosives handbook - properties of chemical explosives and explosive simulants (Lawrence Livemore National Laboratory).

Domasevitch, K.V., Gospodinov, I., Krautscheid, H., Klapötke, T.M., and Stierstorfer, J. (2019). Facile and selective polynitrations at the 4-pyrazolyl dual backbone: straightforward access to a series of high-density energetic materials. New J. Chem. *43*, 1305-1312.

Dong, H., and Zhou, F. (1989). High-Energy Explosives and Related Properties (Science Press).

Du, Y., Wang, Y.H., Li, Y.J., Zheng, Z.H., and Wang, J.L. (2013). Theoretical Calculation of the Detonation Parameters of ANPyO and Comparison between ANPyO and me (ANPyO) x on their Performance. Adv. Mater. Res. *791*, 60-63.

Fischer, D., Gottfried, J.L., Klapötke, T.M., Karaghiosoff, K., Stierstorfer, J., and Witkowski, T.G. (2016). Synthesis and investigation of advanced energetic materials based on bispyrazolylmethanes. Angew. Chem. *128*, 16366-16369.

Fischer, D., Klapötke, T.M., and Stierstorfer, J. (2014). Synthesis and characterization of diaminobisfuroxane. Eur. J. Inorg. Chem. *2014*, 5808-5811.

Fischer, N., Fischer, D., Klapötke, T.M., Piercey, D.G., and Stierstorfer, J. (2012). Pushing the limits of energetic materials–the synthesis and characterization of dihydroxylammonium 5, 5′-bistetrazole-1, 1′-diolate. J. Mater. Chem. *22*, 20418-20422.

Fonger, G.C., Hakkinen, P., Jordan, S., and Publicker, S. (2014). The National Library of Medicine's (NLM) Hazardous Substances Data Bank (HSDB): background, recent enhancements and future plans. Toxicology *325*, 209-216.

Fried, L.E. (1998). LLNL CHEETAH Reactant Library. 1.0 ed.: SANDIA REPORT SAND98-1191, Unlimited Release.

Gao, B., Wang, D., Zhang, J., Hu, Y., Shen, J., Wang, J., Huang, B., Qiao, Z., Huang, H., Nie, F., et al. (2014). Facile, continuous and large-scale synthesis of CL-20/HMX nano co-crystals with high-performance by ultrasonic spray-assisted electrostatic adsorption method. J. Mater. Chem. A *2*, 19969-19974.

Gill, R., Asaoka, L., and Baroody, E. (2006). On underwater detonations, 1. A new method for predicting the CJ detonation pressure of explosives. J. Energ. Mater. *5*, 287-307.

Goebel, M., Klapoetke, T.M., and Mayer, P. (2006). Crystal structures of the potassium and silver salts of nitroform. Z. Anorg. Allg. Chem. *632*, 1043-1050.

Gore, G., Sivabalan, R., Nair, U., Saikia, A., Venugopalan, S., and Gandhe, B. (2007). Synthesis of CL-20: By oxidative debenzylation with cerium (IV) ammonium nitrate (CAN). Indian J. Chem. *46B*, 505-508.

Guillou, S., Jacob, G., Terrier, F., and Goumont, R. (2009). An unexpected synthesis of 7-azidofurazano[3,4-b]tetrazolopyrazine. Tetrahedron *65*, 8891-8895.

Guo, J., Zhang, T., Zhang, J., and Liu, Y. (2006). Experimental Studies on the 2,4,6-Trinitro-m-Xylene Crystal. Chin. J. Explos. Propellants *29*, 58-62.

Hall, R.H., and Wright, G.F. (1951). Reaction of acetyl chloride with 1-nitro-2-nitramino-2-propoxyimidazolidine. J. Am. Chem. Soc. *73*, 2213-2216.

He, Z., Yan, S., and Liu, Z. (2013). Thermal Decomposition Characteristics of 2,6-Diamino-3,5-dinitropyridine-1-oxide. Chin. J. Explos. Propellants *36*, 51.

Headqurters, D.T.A. (1984). Military Explosives (Headqurters department the army).

Hobbs, M.L., and Baer, M.R. (1993) Published. Calibrating the BKW-EOS with a large product species data base and measured C-J properties. 10th Symposium (International) on Detonation, 1993 of Conference Boston, Massachusetts. 409.

Hong, D., Li, Y., Zhu, S., Zhang, L., and Pang, C. (2015). Three insensitive energetic co-crystals of 1-nitronaphthalene, with 2, 4, 6-trinitrotoluene (TNT), 2, 4, 6-trinitrophenol (picric acid) and D-mannitol hexanitrate (MHN). Cent. Eur. J. Energ. Mater. *12*, 47-62.

Huang, H., Shi, Y., Yang, J., and Li, B. (2015). Compatibility study of dihydroxylammonium 5, 5′-bistetrazole-1, 1′-diolate (TKX-50) with some energetic materials and inert materials. J. Energ. Mater. *33*, 66-72.

Huang, H., Zhou, Z., Song, J., Liang, L., Wang, K., Cao, D., Sun, W., Dong, X., and Xue, M. (2011). Energetic salts based on dipicrylamine and its amino derivative. Chemistry–A European Journal *17*, 13593-13602.

Huang, J., Cheng, B., Ma, Q., and Nie, F. (2011). The study of synthesis technology and performance of HNBB. Chin. J. Energ. Mater. *19*, 240.

Huang, Q., Ma, Y., Guo, Z., Liao, L., Hao, S., Nie, F., and Li, H. (2019). An unexpected method to synthesize fluorinated derivative of ANPZ. Propellants, Explos., Pyrotech. *44*, 1521-1527.

Hussein, A.K., Zeman, S., and Elbeih, A. (2018). Synthesis, Performance, and Thermal Behavior of a Novel Insensitive EDNA/DAT Co-crystal. Zeitschrift für anorganische und allgemeine Chemie *644*, 430-437.

Jiao, Q., Zhu, Y., Xing, J., Ren, H., and Huang, H. (2014). Thermal Decomposition of Rdx/Ap by Tg–Dsc–Ms–Ftir. J. Therm. Anal. Calorim. *116*, 1125-1131.

Kamlet, M.J., and Dickinson, C. (1968). Chemistry of detonations. III. Evaluation of the simplified calculational method for chapman-jouguet detonation pressures on the basis of available experimental information. J. Chem. Phys. *48*, 43-50.

Keshavarz, M.H. (2005). Simple procedure for determining heats of detonation. Thermochim. Acta *428*, 95-99.

Keshavarz, M.H. (2007). Detonation velocity of pure and mixed CHNO explosives at maximum nominal density. J. Hazard. Mater. *141*, 536-539.

Keshavarz, M.H. (2007). Quick estimation of heats of detonation of aromatic energetic compounds from structural parameters. J. Hazard. Mater. *143*, 549-554.

Keshavarz, M.H. (2008). Estimating heats of detonation and detonation velocities of aromatic energetic compounds. Propellants, Explos., Pyrotech. *33*, 448-453.

Keshavarz, M.H. (2012). A simple way to predict heats of detonation of energetic compounds only from their molecular structures. Propellants, Explos., Pyrotech. *37*, 93-99.

Keshavarz, M.H., and Pouretedal, H.R. (2005). Predicting the detonation velocity of CHNO explosives by a simple method. Propellants, Explos., Pyrotech. *30*, 105-108.

Kettner, M.A., Karaghiosoff, K., Klapötke, T.M., Sućeska, M., and Wunder, S. (2014). 3, 3′-Bi (1, 2, 4-oxadiazoles) Featuring the Fluorodinitromethyl and Trinitromethyl Groups. Chemistry–A European Journal *20*, 7622-7631.

Khire, V., Talawar, M., Prabhakaran, K., Mukundan, T., and Kurian, E. (2005). Spectro-thermal decomposition study of 1, 4-dinitroglycoluril (DINGU). J. Hazard. Mater. *119*, 63-68.

Kim, S., Chen, J., Cheng, T., Gindulyte, A., He, J., He, S., Li, Q., Shoemaker, B.A., Thiessen, P.A., Yu, B., et al. (2018). PubChem 2019 update: improved access to chemical data. Nucleic Acids Res. *47*, D1102-D1109.

Klapötke, T.M., Mieskes, F., Stierstorfer, J., and Weyrauther, M. (2016). Studies on Energetic Salts Based on (2, 4, 6-Trinitrophenyl) guanidine. Propellants, Explos., Pyrotech. *41*, 217-222.

Klapötke, T.M., Stierstorfer, J., Weyrauther, M., and Witkowski, T.G. (2016). Synthesis and Investigation of 2, 6-Bis (picrylamino)-3, 5-dinitro-pyridine (PYX) and Its Salts. Chemistry–A European Journal *22*, 8619-8626.

Klapötke, T.M., and Witkowski, T.G. (2016). 5, 5′-Bis (2, 4, 6-trinitrophenyl)-2, 2′-bi (1, 3, 4-oxadiazole)(TKX-55): Thermally Stable Explosive with Outstanding Properties. ChemPlusChem *81*, 357-360.

Kofler, A., and Brandstätter, M. (1948). Zur isomorphen vertretbarkeit von H, OH, Cl: S-trinitrobenzol, pikrinsäure, pikrylchlorid. Monatshefte für Chemie und verwandte Teile anderer Wissenschaften *78*, 65-70.

Kumar, D., Tang, Y., He, C., Imler, G.H., Parrish, D.A., and Shreeve, J.N.M. (2018). Multipurpose Energetic Materials by Shuffling Nitro Groups on a 3, 3′-Bipyrazole Moiety. Chemistry–A European Journal *24*, 17220-17224.

Kwasny, M., and Syczewski, M. (1980). Preparation and some physicochemical properties of compounds with trinitromethyl group. Biul. Wojsk. Akad. Tech. Im. Jaroslawa Dabrowskiego *29*, 165-172.

Lange, K., Koenig, A., Roegler, C., Seeling, A., and Lehmann, J. (2009). NO donors. Part 18: Bioactive metabolites of GTN and PETN—Synthesis and vasorelaxant properties. Bioorg. Med. Chem. Lett. *19*, 3141-3144.

Lee, J., Hsu, C., and Chang, C. (2002). A study on the thermal decomposition behaviors of PETN, RDX, HNS and HMX. Thermochim. Acta *392*, 173-176.

Lee, P.P., and Back, M.H. (1986). Kinetic studies of the thermal decomposition of tetryl using accelerating rate calorimetry: part I. Derivation of the activation energy for decomposition. Thermochim. Acta *107*, 1-16.

Leemann, H., and Grandmougin, E. (1908). Zur Kenntnis des symm. Hexanitro-azobenzols. Ber. Dtsch. Chem. Ges. *41*, 1295-1305.

Leonard, N.J., Miller, L.A., and Thomas, P.D. (1956). Unsaturated amines. VIII. Dehydrogenation and hydroxylation of 1-methyldecahydroquinoline by means of mercuric acetate1. J. Am. Chem. Soc. *78*, 3463-3468.

Leonard, P.W., Pollard, C.J., Chavez, D.E., Rice, B.M., and Parrish, D.A. (2011). 3, 6-Bis (4-nitro-1, 2, 5-oxadiazol-3-yl)-1, 4, 2, 5-dioxadiazene (BNDD): A Powerful Sensitive Explosive. Synlett *22*, 2097-2099.

Lewis, R.J., and Sax, N. (1996). Sax's dangerous properties of industrial materials (New York).

Li, B., Dong, H., and Zhang, J. (2003). Thermal Properties of Main By-products in TATB. Chin. J. Energ. Mater. *11*, 85-87.

Li, C., Liang, L., Wang, K., Bian, C., Zhang, J., and Zhou, Z. (2014). Polynitro-substituted bispyrazoles: a new family of high-performance energetic materials. J. Mater. Chem. A *2*, 18097-18105.

Li, H., An, C., Wen, X., Wang, J., and Du, M. (2016). Study on kinetic parameters of thermal decomposition reaction and thermal stability of 3, 4-bis (3-nitrofurazan-4-yl) furoxan based on kissinger method. Chin. J. Explos. Propellants *39*, 58-65.

Li, H., Li, D., Zeng, X., Liu, K., Beckers, H., Schaefer Iii, H.F., Esselman, B.J., and Mcmahon, R.J. (2015). Toward Understanding the Decomposition of Carbonyl Diazide (N3) 2CO and Formation of Diazirinone cycl-N2CO: Experiment and Computations. J. Phys. Chem. A *119*, 8903-8911.

Li, H., Zhang, L., Petrutik, N., Wang, K., Ma, Q., Shem-Tov, D., Zhao, F., and Gozin, M. (2019). Molecular and crystal features of thermostable energetic materials: guidelines for architecture of "bridged" compounds. ACS Cent. Sci. *6*, 54-75.

Li, W., Li, Z., and Wang, W. (2009). Preparation and Properties of TOATF. Chin. J. Energ. Mater. *17*, 11-13.

Licht, H., and Ritter, H. (1988). 2, 4, 6 - Trinitropyridine and Related Compounds, synthesis and characterization. Propellants, Explos., Pyrotech. *13*, 25-29.

Liu, L., Jin, X., Wang, P., Zhou, X., and Lu, M. (2016). Synthesis Improvement and Thermal Properties of Bis(2,2,2-Trinitroethyl)-Nitramine (BTNNA). Explos. Mater. *45*, 47-50.

Liu, L., Zhang, Y., Zhang, S., and Fei, T. (2015). Heterocyclic Energetic Salts of 4, 4′, 5, 5′-Tetranitro-2, 2′-Biimidazole. J. Energ. Mater. *33*, 202-214.

Liu, N., Shu, Y., Li, H., Zhai, L., Li, Y., and Wang, B. (2015). Synthesis, characterization and properties of heat-resistant explosive materials: polynitroaromatic substituted difurazano [3, 4-b: 3′, 4′-e] pyrazines. RSC Adv. *5*, 43780-43785.

Liu, N., Wang, B., Liu, H., Li, Y., Huo, H., Zhai, L., and Lai, W. (2015). Synthesis Crystal Structure and Thermal Properties of Two Furazano [3,4-b] tetrazolo [1,2-d] pyrazines. Chin. J. Energ. Mater. *23*, 13-17.

Makhova, N.N., Epishina, M.A., Ovchinnikov, I.V., and Pivina, T.S. (2003). New macrocyclic systems containing difurazanyl and furazanofuroxanyl units. Int. Annu. Conf. ICT *34th*, 80.

Manelis, G., Nazin, G., and Prokudin, V. (2006) Published. The additional activation volume of unimolecular reactions in the solid phase. Doklady Physical Chemistry, 2006 of Conference.: Springer, 335-338.

Mcneil, S.K., Kelley, S.P., Beg, C., Cook, H., Rogers, R.D., and Nikles, D.E. (2013). Cocrystals of 10-methylphenthiazine and 1, 3-dinitrobenzene: implications for the optical sensing of TNT-based explosives. ACS Appl. Mater. Interfaces *5*, 7647-7653.

Meyer, R., Köhler, J., and Homburg, A. (2016). Explosives (John Wiley & Sons).

Meyer, R., Köhler, J., and Homburg, D.I.A. (2007). Explosives (Wiley - VCH Verlag GmbH & Co. KGaA).

Mo, Z., Zhang, A., Cao, X., Liu, Q., Xu, X., An, H., Pei, W., and Zhu, S. (2010). JASMIN: a parallel software infrastructure for scientific computing. Front. Comput. Sci. China *4*, 480–488.

Nair, U., Gore, G., Sivabalan, R., Pawar, S., Asthana, S., and Venugopalan, S. (2007). Preparation and

thermal studies on tetranitrodibenzo tetraazapentalene (TACOT): A thermally stable high explosive. J. Hazard. Mater. *143*, 500-505.

Nielsen, A.T., Atkins, R.L., and Norris, W.P. (1979). Oxidation of poly (nitro) anilines to poly (nitro) benzenes. Synthesis of hexanitrobenzene and pentanitrobenzene. J. Org. Chem. *44*, 1181-1182.

Ohta, A., Ogihara, Y., Nei, K., and Shibata, S. (1963). On Methylphenylnaphthalenes. I. Syntheses of Methylphenylnaphthalenes. Chem. Pharm. Bull. *11*, 754-758.

Pepekin, V., Matyushin, Y.N., and Gubina, T. (2011). Enthalpy of formation and explosive properties of 5, 6-(3, 4-furazano)-1, 2, 3, 4-tetrazine-1, 3-dioxide. Russ. J. Phys. Chem. B *5*, 97.

Politzer, P., and Murray, J.S. (2011). Some perspectives on estimating detonation properties of C, H, N, O compounds. Cent. Eur. J. Energ. Mater. *8*, 209-220.

Qu, Y., and Babailov, S.P. (2018). Azo-linked high-nitrogen energetic materials. J. Mater. Chem. A *6*, 1915-1940.

Rice, B.M., and Hare, J. (2002). Predicting heats of detonation using quantum mechanical calculations. Thermochim. Acta *384*, 377-391.

Rieckmann, T., Völker, S., Lichtblau, L., and Schirra, R. (2001). Investigation on the thermal stability of hexanitrostilbene by thermal analysis and multivariate regression. Chem. Eng. Sci. *56*, 1327-1335.

Roháč, M., Zeman, S., and RůŽičKa, A. (2008). Crystallography of 2, 2′, 4, 4′, 6, 6′-Hexanitro-1, 1′-biphenyl and Its Relation to Initiation Reactivity. Chem. Mater. *20*, 3105-3109.

Rothstein, L.R., and Petersen, R. (1979). Predicting high explosive detonation velocities from their composition and structure. Propellants, Explos., Pyrotech. *4*, 56-60.

Saraf, S., Rogers, W., and Mannan, M.S. (2003). Prediction of reactive hazards based on molecular structure. J. Hazard. Mater. *98*, 15-29.

Šarlauskas, J. (2010). Polynitrobenzenes containing alkoxy and alkylenedioxy groups: potential HEMs and precursors of new energetic materials. Cent. Eur. J. Energ. Mater. *7*, 313-324.

Schmidt, J., and Gehlen, H. (1965). PK-werte von derivaten des 1, 2, 4-triazols. Zeitschrift für Chemie *5*, 304-304.

Sheremetev, A.B., Kulagina, V.O., Aleksandrova, N.S., Dmitriev, D.E., Strelenko, Y.A., Lebedev, V.P., and Matyushin, Y.N. (1998). Dinitro trifurazans with oxy, azo, and azoxy bridges. Propellants, Explos., Pyrotech. *23*, 142-149.

Sheremetev, A.B., Kulagina, V.O., and Ivanova, E.A. (1996). Zero-hydrogen furazan macrocycles with oxy and azo bridges. J. Org. Chem. *61*, 1510-1511.

Sheremetev, A.B., Lyalin, B.V., Kozeev, A.M., Palysaeva, N.V., Struchkova, M.I., and Suponitsky, K.Y. (2015). A practical anodic oxidation of aminofurazans to azofurazans: an environmentally friendly route. RSC Adv. *5*, 37617-37625.

Siele, V., and Warman, M. (1962). Preparation of 1, 3-Difluoro-2, 4, 6-trinitrobenzene. J. Org. Chem. *27*, 1910-1911.

Sikder, N., Sikder, A., Bulakh, N., and Gandhe, B. (2004). 1, 3, 3-Trinitroazetidine (TNAZ), a melt-cast explosive: synthesis, characterization and thermal behaviour. J. Hazard. Mater. *113*, 35-43.

Sinditskii, V., Burzhava, A., Chernyi, A., Shmelev, D., Apalkova, V., Palysaeva, N., and Sheremetev, A. (2016). A comparative study of two difurazanyl ethers. J. Therm. Anal. Calorim. *123*, 1431-1438.

Singh, A., Sikder, N., and Sikder, A.K. (2005). Improved synthesis of an energetic material, 1, 3, 3-

trinitroazetidine (TNAZ) exploiting 2-iodoxy benzoic acid (IBX) as an oxidising agent. Indian J. Chem. *44B*, 2560-2563.

Spencer, E., and Wright, G.F. (1946). Preparation of picramide. Can. J. Res. *24*, 204-207.

Srinivasan, P., Gunasekaran, M., Kanagasekaran, T., Gopalakrishnan, R., and Ramasamy, P. (2006). 2, 4, 6-trinitrophenol (TNP): An organic material for nonlinear optical (NLO) applications. J. Cryst. Growth *289*, 639-646.

Tang, Y., He, C., Imler, G.H., Parrish, D.A., and Jean'ne, M.S. (2018). Ring closure of polynitroazoles via an N, N′-alkylene bridge: towards high thermally stable energetic compounds. J. Mater. Chem. A *6*, 8382-8387.

Tang, Y., He, C., Imler, G.H., Parrish, D.A., and Jean’ne, M.S. (2018). AC–C bonded 5, 6-fused bicyclic energetic molecule: exploring an advanced energetic compound with improved performance. Chem. Commun. *54*, 10566-10569.

Tang, Y., Kumar, D., and Shreeve, J.N.M. (2017). Balancing excellent performance and high thermal stability in a dinitropyrazole fused 1, 2, 3, 4-tetrazine. J. Am. Chem. Soc. *139*, 13684-13687.

Taylor, H.A., and Vesselovsky, V.V. (2002). The thermal decomposition of nitromethane. J. Phys. Chem. *39*, 1095-1102.

Terrier, F., Xie, H.Q., and Farrell, P.G. (1990). The effect of nitro-substitution upon diphenylmethane reactivity. J. Org. Chem. *55*, 2610-2616.

Tian, D., Zhao, F., and Liu, J. (2011). Handbook of energetic materials and the related compounds (National Defense Industry Press).

Trotter, J. (1960). The crystal structure of 1, 5-dinitronaphthalene. Acta Crystallogr. *13*, 95-99.

Tsyshevsky, R., Pagoria, P., Smirnov, A.S., and Kuklja, M.M. (2017). Comprehensive end-to-end design of novel high energy density materials: II. Computational modeling and predictions. J. Phys. Chem. C *121*, 23865-23874.

Türker, L. (2012). A trigonometric approach to a limiting law on detonation velocity. Match-Communications in Mathematical and Computer Chemistry *67*, 127.

Ulpiani, C. (1912). Constitution of Fulminuric Acids. IV. Compounds of the Formula H2(C2N2O3). Gazz. Chim. Ital. *42*, 243-63.

Veauthier, J.M., Chavez, D.E., Tappan, B.C., and Parrish, D.A. (2010). Synthesis and characterization of furazan energetics ADAAF and DOATF. J. Energ. Mater. *28*, 229-249.

Volk, F., and Bathelt, H. (1997). Influence of energetic materials on the energy-output of gun propellants. Propellants, Explos., Pyrotech. *22*, 120-124.

Wang, G., Xiao, H., Ju, X., and Gong, X. (2006). Calculation of detonation velocity, pressure, and electric sensitivity of nitro arenes based on quantum chemistry. Propellants, Explos., Pyrotech. *31*, 361-368.

Wang, G., Xiao, H., Xu, X., and Ju, X. (2006). Detonation velocities and pressures, and their relationships with electric spark sensitivities for nitramines. Propellants, Explos., Pyrotech. *31*, 102-109.

Wang, H., Wang, Y., Li, Y., Liu, Y., and Tan, Y. (2014). Scale-up synthesis and characterization of 2, 6-diamino-3, 5-dinitropyrazine-1-oxide. Def. Technol. *10*, 343-348.

Wang, Y., Yang, Z., Li, H., Zhou, X., Zhang, Q., Wang, J., and Liu, Y. (2014). A novel cocrystal explosive of HNIW with good comprehensive properties. Propellants, Explos., Pyrotech. *39*, 590-596.

Wei, J., Li, F., Xu, J., and Peng, X. (2015). Synthesis and thermal stability of new polynitrostilbenes.

Aust. J. Chem. *68*, 919-925.

Wikipedia. 2006. Kamlet-Jacobs-Gleichungen [Online]. Available: https://de.wikipedia.org/wiki/Kamlet-Jacobs-Gleichungen.

Wu, J., Zhang, J., Li, T., Li, Z., and Zhang, T. (2015). A novel cocrystal explosive NTO/TZTN with good comprehensive properties. RSC Adv. *5*, 28354-28359.

Wurzenberger, M.H., Lechner, J.T., Lommel, M., Klapötke, T.M., and Stierstorfer, J. (2020). Salts of Picramic Acid–Nearly Forgotten Temperature-Resistant Energetic Materials. Propellants, Explos., Pyrotech.

Yan, T., Cheng, G., and Yang, H. (2019). 1, 2, 4-Oxadiazole-Bridged Polynitropyrazole Energetic Materials with Enhanced Thermal Stability and Low Sensitivity. ChemPlusChem *84*, 1567-1577.

Yang, C.H., Lu, Y.M., Yan, M.Q., Li, J., Wu, J., Li, Q.Y., Yang, J., Shen, L., Yang, G.W., and Zou, J.H. (2016). Nitrogen–rich 1, 2-bis (tetrazol-5-yl) ethane and its Carboxylate Derivative for Potential Energetic Materials. ChemistrySelect *1*, 2757-2761.

Yang, Z., Li, H., Zhou, X., Zhang, C., Huang, H., Li, J., and Nie, F. (2012). Characterization and properties of a novel energetic–energetic cocrystal explosive composed of HNIW and BTF. Cryst. Growth Des. *12*, 5155-5158.

Yang, Z., Zeng, Q., Zhou, X., Zhang, Q., Nie, F., Huang, H., and Li, H. (2014). Cocrystal explosive hydrate of a powerful explosive, HNIW, with enhanced safety. RSC Adv. *4*, 65121-65126.

Yin, P., and Shreeve, J.N.M. (2015). From N-Nitro to N-Nitroamino: Preparation of High-Performance Energetic Materials by Introducing Nitrogen-Containing Ions. Angew. Chem. *127*, 14721-14725.

Yin, P., Zhang, J., Imler, G.H., Parrish, D.A., and Shreeve, J.N.M. (2017). Polynitro-Functionalized Dipyrazolo-1, 3, 5-triazinanes: Energetic Polycyclization toward High Density and Excellent Molecular Stability. Angew. Chem. *129*, 8960-8964.

Yin, P., Zhang, J., Parrish, D.A., and Jean'ne, M.S. (2014). Energetic N, N′-Ethylene-Bridged Bis (nitropyrazoles): Diversified Functionalities and Properties. Chemistry–A European Journal *20*, 16529-16536.

Zaitsev, A., Kortusov, I., Dalinger, I., Kachala, V., Popova, G., and Shevelev, S. (2009). Nitropyrazoles 16. The use of methoxymethyl group as a protecting group for the synthesis of 4-methyl-3-nitro-5-R-pyrazoles. Russ. Chem. Bull. *58*, 2118-2121.

Zeman, S. (1980). Possibilities of applying Piloyan method of determination of decomposition activation energies in differential thermal analysis of polynitroaromatic compounds and their derivatives: Part IV. 1, 3, 5-trinitrobenzene, 2, 2′, 4, 4′, 6, 6′-hexanitrobiphenyl, 2, 2′, 2 ″, 4, 4′, 4 ″, 6, 6′, 6 ″-nonanitro-m-terphenyl, 1, 4, 5, 8-tetranitronaphthalene and 2, 4, 6-tripicryl-l, 3, 5-triazine. J. Therm. Anal. Calorim. *19*, 207-214.

Zeman, S. (1993). The thermoanalytical study of some aminoderivatives of 1, 3, 5-trinitrobenzene. Thermochim. Acta *216*, 157-168.

Zeman, S. (2003). New aspects of impact reactivity of polynitro compounds. Part IV. Allocation of polynitro compounds on the basis of their impact sensitivities. Propellants, Explos., Pyrotech. *28*, 308-313.

Zeman, S., Roháč, M., Friedl, Z., Růžička, A., and Lyčka, A. (2010). Crystallography and Structure–Property Relationships of 2, 2 ″, 4, 4′, 4 ″, 6, 6′, 6 ″-Octanitro-1, 1′: 3′, 1 ″-Terphenyl (ONT).

Propellants, Explos., Pyrotech. *35*, 130-135.
Zeng, Z., Guo, Y., Twamley, B., and Jean'ne, M.S. (2009). Energetic polyazole polynitrobenzenes and their coordination complexes. Chem. Commun., 6014-6016.
Zhang, H., Guo, C., Wang, X., Xu, J., He, X., Liu, Y., Liu, X., Huang, H., and Sun, J. (2013). Five energetic cocrystals of BTF by intermolecular hydrogen bond and π-stacking interactions. Cryst. Growth Des. *13*, 679-687.
Zhang, J., Wang, J., Xu, H., and Zhou, X. (2013). Synthesis and thermal decomposition kinetics of hexanitroazobenzene. Chin. J. Energ. Mater. *21*, 7-11.
Zhang, J., and Xiao, H. (2002). Computational studies on the infrared vibrational spectra, thermodynamic properties, detonation properties, and pyrolysis mechanism of octanitrocubane. J. Chem. Phys. *116*, 10674-10683.
Zhang, J., Xue, B., Rao, G., Chen, L., and Chen, W. (2018). Thermal decomposition characteristic and kinetics of DINA. J. Therm. Anal. Calorim. *133*, 727-735.
Zhang, L., Jiang, S.-L., Yu, Y., Long, Y., Zhao, H.-Y., Peng, L.-J., and Chen, J. (2016). Phase Transition in Octahydro-1,3,5,7-tetranitro-1,3,5,7-tetrazocine (HMX) under Static Compression: An Application of the First-Principles Method Specialized for CHNO Solid Explosives. J. Phys. Chem. B *120*, 11510-11522.
Zhang, P., Kumar, D., Zhang, L., Shem-Tov, D., Petrutik, N., Chinnam, A.K., Yao, C., Pang, S., and Gozin, M. (2019). Energetic Butterfly: Heat-Resistant Diaminodinitro trans-Bimane. Molecules *24*, 4324.
Zhang, X., Dong, H., Zhou, Z., and Li, H. (2010). Synthesis and Properties of 3-Amino-2,4,6-Trinitrophenol and 3,5-Diamino-2,4,6-Trinitrophenol. Acta Armamentarii *31*, 1341-1345.
Zhang, X., Xiong, H., Yang, H., and Cheng, G. (2017). 1 4, 1 6, 3 4, 3 6, 5 4, 5 6, 7 4, 7 6-Octanitro-2, 4, 6, 8-tetraoxa-1, 3, 5, 7 (1, 3)-tetrabenzenacyclooctaphane and its derivatives: thermally stable explosives with outstanding properties. New J. Chem. *41*, 5764-5769.
Zhang, Y., Zhou, C., Wang, B., Zhou, Y., Xu, K., Jia, S., and Zhao, F. (2014). Synthesis and Characteristics of Bis (nitrofurazano) furazan (BNFF), an Insensitive Material with High Energy - Density. Propellants, Explos., Pyrotech. *39*, 809-814.
Zhao, X., and Liu, Z. (2013). 2, 6-Diamino-3, 5-dinitropyrazine-1-oxide synthesis and its explosion properties. J. Chem. Eng. Chin. Univ. *2*, 248.
Zhou, Y., Wang, B., Li, J., Zhou, C., Hu, L., Chen, Z., and Zhang, Z. (2011). Study on Synthesis, Characterization and Properties of 3,4-Bis(4'-nitrofurazano-3'-yl)furoxan. Acta Chim. Sin. (Chin. Ed.) *69*, 1673-1680.